Inorganic Chemistry

pubs.acs.org/IC Article

Triazole-Based Half-Sandwich Ruthenium(II) Compounds: From *In Vitro* Antiproliferative Potential to *In Vivo* Toxicity Evaluation

Oscar A. Lenis-Rojas,* Rui Cabral, Beatriz Carvalho, Sofia Friães, Catarina Roma-Rodrigues, Jhonathan A. A. Fernández, Sabela F. Vila, Laura Sanchez, Clara S. B. Gomes, Alexandra R. Fernandes,* and Beatriz Royo*

Cite This: *Inorg. Chem.* 2021, 60, 8011−8026 Read Online

ACCESS | Metrics & More | Article Recommendations | Supporting Information

ABSTRACT: A new series of half-sandwich ruthenium(II) compounds $[(\eta^6\text{-arene})Ru(L)Cl][CF_3SO_3]$ bearing 1,2,3-triazole ligands (arene = *p*-cymene, L = **L1** (**1**); arene = *p*-cymene, L = **L2** (**2**); arene = benzene, L = **L1** (**3**); arene = benzene, **L2** (**4**); **L1** = 2-[1-(*p*-tolyl)-1*H*-1,2,3-triazol-4-yl]pyridine and **L2** = 1,1′-di-*p*-tolyl-1*H*,1′*H*-4,4′-bi(1,2,3-triazole) have been synthesized and fully characterized by ^{1}H and ^{13}C NMR and IR spectroscopy, mass spectrometry, and elemental analysis. The molecular structures of **1**, **2**, and **4** have been determined by single-crystal X-ray diffraction. The cytotoxic activity of **1**−**4** was evaluated using the MTS assay against human tumor cells, namely ovarian carcinoma (A2780), colorectal carcinoma (HCT116), and colorectal carcinoma resistant to doxorubicin (HCT116dox), and against normal primary fibroblasts. Whereas compounds **2** and **4** showed no cytotoxic activity toward tumor cell lines, compounds **1** and **3** were active in A2780, while showing no antiproliferative effect in human normal dermal fibroblasts at the IC_{50} concentrations of the A2780 cell line. Exposure of ovarian carcinoma cells to IC_{50} concentrations of compound **1** or **3** led to an accumulation of reactive oxygen species and an increase of apoptotic and autophagic cells. While compound **3** displayed low levels of angiogenesis induction, compound **1** showed an ability to induce cell cycle delay and to interfere with cell migration. When the *in vivo* toxicity studies using zebrafish and chicken embryos are considered, compounds **1** and **3**, which were not lethal, are promising candidates as anticancer agents against ovarian cancer due to their good cytotoxic activity in tumor cells and their low toxicity both *in vitro* and *in vivo*.

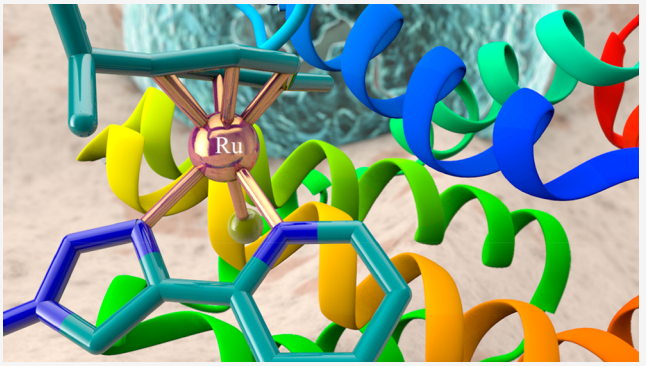

INTRODUCTION

Cancer is a group of diseases with an enormous socioeconomic burden, being the second leading cause of death worldwide.[1] In fact, the growth in oncology cost is constantly increasing.[2] Chemotherapy represents the most effective and broadly used modality in most types of cancers.[3] Since the introduction of the metallic chemotherapeutic cisplatin and other platinum drugs, the cure rate improved in most types of cancer.[4] However, the clinical use of platinum-based anticancer drugs is limited by their severe side effects and inherent or acquired resistance of tumors to the treatment.[4,5] Currently, new metal agents other than platinum have been investigated as antitumor agents.[6] In particular, Ru, Ir, Os, and Au complexes have emerged as promising alternatives to platinum-based drugs.[6] The objective is to develop metallodrugs that interact with DNA differently from classical platinum drugs or whose mode of action involve other targets such as proteins and enzymes, leading to efficient tumor cell death pathways. Moreover, the application of metallodrugs that surpass the acquired resistance mechanisms of tumor cells to cisplatin, including metal compounds with higher drug uptake and lower efflux, is highly valuable.[7] In particular, some ruthenium compounds have exhibited very promising antiproliferative activity, being less toxic than platinum drugs.[8] The ruthenium compound NKP1339 (Scheme 1) has shown high *in vitro* and *in vivo* antitumor activity, reaching clinical trials for advanced solid tumors (NCT01415297).[8−11] In addition, the arene ruthenium based complexes RM175 and RAPTA-C are currently in the preclinical stage (Scheme 1).[12−17] Despite the fact that RAPTA-C generally has shown low cytotoxicity *in vitro*,[13,14] it displays important antimetastatic and antiangiogenic properties *in vivo*.[15] Although the complete mechanism of action of the RAPTA class of compounds is unknown, unlike the case for classical platinum-based anticancer agents, RAPTA-C binds to the core of the histone protein in

Received: February 21, 2021
Published: May 11, 2021

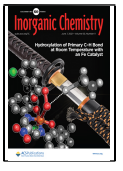

Scheme 1. Chemical Structures of NKP1339, RAPTA-C, and RM175

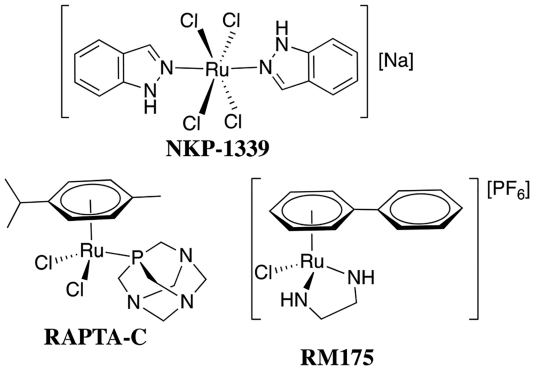

chromatin and not to DNA,[15] which can explain its intrinsic antiangiogenic activity.[15] In contrast, the arene ruthenium RM175 has been shown to reduce the growth of primary tumors through strong DNA interactions with guanines,[15] and its mechanism of action is based on the induction of apoptosis through Bax and p53 pathways.[17] RM175 also exerts activity by interrupting the processes of cell invasion and migration.

Despite the promising pharmacological properties of ruthenium(II) arene compounds, further development of Ru-based compounds with desirable biological properties is needed to successfully promote these compounds as promising chemotherapeutic candidates. The rational design of the ancillary ligands has resulted in success in the development of anticancer complexes, including the introduction of bidentate ligands with donor atoms of different nature in $[Ru(\eta^6\text{-arene})(L)X]^{n+}$ complexes (L = bidentate ligand, X = halogen).[18] The use of N^N chelating ligands has been one of the most widely used strategies to tune the anticancer properties of $[Ru(\eta^6\text{-arene})(L)X]^{n+}$ complexes.[19−25] However, among chelating N^N ligands, the use of 1,2,3-triazoles have received little attention. Kandioller and co-workers recently reported the anticancer activity of a series of cyclometalated 1,2,3-triazole-derived ruthenium(II) complexes with a variety of substituted triazoles,[26] bearing different N- and S-donor leaving groups (Scheme 2).[27] Investigations on their mechanism of action revealed that this class of Ru complexes is an inducer of apoptosis but has no DNA intercalation.[27] In addition, Makhubela and co-workers proved that this kind of complex binds to human albumin (Scheme 2).[28] The anticancer activity studies of these ruthenium metallacycles have been limited to *in vitro* studies.

Scheme 2. Half-Sandwich Ru(II) Complexes with Cyclometalated 1,2,3-Triazole, N^C Ligands Explored as Anticancer Agents

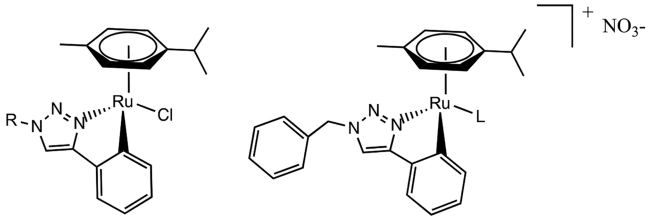

Intrigued by the activities of organometallic complexes with triazole-derived ligands, and in a continuation of our interest in developing Ru-based anticancer drugs,[8−11] herein we report the anticancer activity of four new chelating N^N Ru(II) arene compounds bearing ditriazole and mixed triazole-pyridine ligands. The effect of the presence of triazole, pyridine rings, and arene (*p*-cymene and benzene) units in the biological activity of the ruthenium compounds has been investigated. Biological studies include *in vitro* cytotoxicity studies of **1**−**4** in ovarian, colon, and colon-resistant cancer cells and in fibroblasts to evaluate the selectivity toward tumor cells and *in vivo* studies using zebrafish and chicken egg models. In addition, the mechanism of cell death in ovarian cancer cells has been investigated.

EXPERIMENTAL SECTION

Materials and Methods. All syntheses were carried out under a nitrogen atmosphere using current Schlenk techniques, and the solvents used were dried prior to use by standard methods.[29] Ligands **L1** and **L2** were synthesized according to literature procedures.[30,31] All other reagents were purchased from commercial suppliers and used without further purification. ^{1}H and ^{13}C NMR spectra were recorded on a Bruker Avance III 400 MHz spectrometer. IR spectra were recorded as Nujol mulls, polyethylene-disk Nujol mulls, or KBr disks on a Satellite FTIR instrument. The FAB mass spectra were recorded using a FISONS Quatro mass spectrometer with a Cs ion gun; 3-nitrobenzyl alcohol was used as the matrix. Elemental analyses were carried out using a Leco TruSpec Micro Elemental Analyzer at the ITQB laboratory.

Synthetic Procedures. *Preparation of [Ru(η^6-p-cymene)(**L1**)-Cl][CF_3SO_3] (**1**).* To a solution of $[Ru(\eta^6\text{-}p\text{-cymene})Cl(\mu\text{-}Cl)]_2$ (0.200 g, 0.326 mmol) in dichloromethane (20 mL) was added $AgCF_3SO_3$ (0.168 g, 0.653 mmol), and the mixture was stirred for 2 h at room temperature. Then, **L1** (0.154 g, 0.653 mmol) was added, and the mixture was stirred overnight at room temperature. The resulting solution was filtered twice through Celite to remove the silver chloride that formed. The solvent was removed from the filtrate under vacuum, and the resulting solid was recrystallized from dichloromethane/*n*-hexane to give **1** as a crystalline yellow solid. Yield: 95% (0.203 g). Anal. Found: C, 45.60; H, 3.96; N, 8.41; S, 4.65. Calcd for $C_{25}H_{26}ClF_3N_6O_3RuS$: C, 45.77; H, 3.99; N, 8.54; S, 4.89. IR (ν_{max}/cm^{-1}): 1249s, 1226sh, 1140s, 1027s [$\nu(CF_3SO_3)$]. ^{1}H NMR (400 MHz, CD_2Cl_2, δ ppm, *J* in Hz): δ_H 9.33 (s, 1H, H_{17}), 9.22 (d, *J*(HH) = 5.4, 1H, H_{11}), 8.26 (d, *J*(HH) = 7.7, 1H, H_{14}), 8.06 (t, *J*(HH) = 6.5, 1H, H_{13}), 7.87 (d, *J*(HH) = 8.3, 2H, H_{19} and H_{24}], 7.58 (t, *J*(HH) = 6.5, 1H, H_{12}), 7.46 (d, *J*(HH) = 8.1, 2H, H_{20} and H_{23}), 5.93 (m, 2H, H_4), 5.89 (d, *J*(HH) = 5.9, 1H, H_9), 5.74 (d, *J* = 6.1 Hz, 1H, H_{10}), 5.70 (d, *J* = 6.1 1H, H_3), 2.82 (m, 1H, H_6), 2.48 (s, 3H, H_{22}), 2.24 (s, 3H, H_1), 1.21 (d, *J*(HH) = 6.9, 3H, H_7), 1.17 (d, *J*(HH) = 6.9, 3H, H_8). ^{13}C NMR (400 MHz, CD_2Cl_2, δ ppm): δ_C 155.2 (C_{11}), 148.6 (C_{15}), 147.6 (C_{16}), 141.8 (C_{21}), 140.5 (C_{13}), 134.0 (C_{18}), 134.1 (C_{20},C_{23}), 131.1 (C_{12}), 123.7 (C_{14}), 123.2 (C_{17}), 121.0 (C_{19},C_{24}), 105.9 (C_5), 102.7 (C_2), 86.7 (C_4), 85.2 (C_9), 84.4 (C_3), 83.7 (C_{10}), 31.5 (C_6), 22.5 (C_8), 21.9 (C_7), 21.4 (C_{22}), 19.9 (C_1). MS-FAB: *m*/*z* 507.0, [Ru(*p*-cymene)(**L1**)Cl]$^+$; 472, [Ru(*p*-cymene)(**L1**)]$^+$.

*Preparation of [Ru(η^6-p-cymene)(**L2**)Cl][CF_3SO_3] (**2**).* Compound **2** was obtained by following a procedure similar to that for **1**. Yield: 95% (0.228 g). Anal. Found: C, 47.36; H, 4.09; N, 11.33; S, 4.15. Calcd for $C_{29}H_{30}ClF_3N_6O_3RuS$: C, 47.31; H, 4.11; N, 11.42; S, 4.35. IR (ν_{max}/cm^{-1}): 1256s, 1222sh, 1151s, 1027s [$\nu(CF_3SO_3)$]. ^{1}H NMR (400 MHz, CD_2Cl_2, δ ppm, *J* in Hz): δ_H 9.38 (s, 2H, H_9), 7.79 (d, *J*(HH) = 8.3, 4H, H_{11}), 7.39 (d, *J*(HH) = 8.2, 4H, H_{12}), 5.91 (d, *J*(HH) = 6.0, 2H, H_4), 5.68 (d, *J*(HH) = 6.0, 2H, H_3), 3.04 (m, 1H, H_6), 2.45 (s, 6H, H_{14}), 2.35 (s, 3H, H_1), 1.33 (d, *J*(HH) = 6.9, 6H, H_7). ^{13}C NMR (400 MHz, CD_2Cl_2, δ ppm): δ_C 141.0 (C_{13}), 139.6 (C_8), 133.9 (C_{10}), 130.8 (C_{12}), 122.4 (C_9), 120.7 (C_{11}), 105.4 (C_5), 101.7 (C_2), 85.8 (C_4), 83.0 (C_3), 31.2 (C_6), 22.4 (C_7), 21.4 (C_{14}),

https://doi.org/10.1021/acs.inorgchem.1c00527
Inorg. Chem. 2021, 60, 8011−8026

19.0 (C_1). MS-FAB: m/z 587.0, [Ru(*p*-cymene)(**L2**)Cl]$^+$; 551.0 [Ru(*p*-cymene)(**L2**)]$^+$.

*Preparation of [Ru(η^6-benzene)(**L1**)Cl][CF_3SO_3] (**3**).* To a solution of [Ru(η^6-benzene)(Cl)(μ-Cl)]$_2$ (0.200 g, 0.326 mmol) in acetone (20 mL) was added $AgCF_3SO_3$ (0.168 g, 0.654 mmol), and the mixture was stirred for 3 h at room temperature. Then, **L1** (0.206 g, 0.652 mmol) was added, and the mixture was stirred overnight at room temperature. The resulting solution was filtered twice through Celite to remove the silver chloride that formed, and the solvent was removed from the filtrate under vacuum to give a solid, which was recrystallized from dichloromethane/*n*-hexane, affording **3** as a green crystalline solid. Yield: 90% (176.0 mg). Anal. Found: C, 42.08; H, 3.02; N, 9.18; S, 5.24. Calcd for $C_{21}H_{18}ClF_3N_4O_3RuS$: C, 42.04; H, 3.02; N, 9.34; S, 5.34. IR (ν_{max}/cm^{-1}): 1246s, 1224sh, 1141s, 1030s [$\nu(CF_3SO_3)$]. ^{1}H NMR (400 MHz, DMSO, δ ppm, J in Hz): δ_H 9.85 (s, 1H, H_8), 9.62 (d, J(HH) = 5.4, 1H, H_2), 8.31 (t, J(HH) = 7.8, 1H, H_5), 8.17 (d, J(HH) = 7.3, 2H, H_4), 7.95 (d, J(HH) = 7.3, 2H, H_{10} and H_{15}), 7.74 (t, J(HH) = 6.0, 1H, H_3), 7.57 (d, J(HH) = 7.7, 2H, H_{11} and H_{14}), 6.24 (s, 6H, H_1), 2.46 (s, 3H, H_{13}). ^{13}C NMR (400 MHz, DMSO, δ ppm): δ_C 156.1 (C_2), 147.7 (C_6), 146.8 (C_7), 140.6 (C_4,C_{12}), 133.4 (C_9), 130.6 (C_{11},C_{14}), 126.1 (C_3), 123.5 (C_8), 122.2 (C_5), 120.7 (C_{10},C_{15}), 86.2 (C_1), 20.73 (C_{13}). MS-FAB: m/z 450.9, [Ru(η^6-benzene)(**L1**)Cl]$^+$; 416.0 [Ru(η^6-benzene)(**L1**)]$^+$.

*Preparation of [Ru(η^6-benzene)(**L2**)Cl][CF_3SO_3] (**4**).* Compound **4** was obtained by following a procedure similar to that for **3**. Yield: 81% (0.179 g). Anal. Found: C, 43.75; H, 3.41; N, 12.09; S, 4.67. Calcd for $C_{25}H_{22}ClF_3N_6O_3RuS$: C, 44.15; H, 3.26; N, 12.36; S, 4.71. IR (ν_{max}/cm^{-1}): 1259s, 1223sh, 1153s, 1028s [$\nu(CF_3SO_3)$]. ^{1}H NMR (400 MHz, CD_2Cl_2, δ ppm, J in Hz): δ_H 9.29 (s, 2H, H_3), 7.83 (d, J(HH) = 8.5, 4H, H_5), 7.45 (d, J(HH) = 8.2, 4H, H_6), 6.07 (s, 6H, H_1), 2.48 (s, 3H, Me_8). ^{13}C NMR (400 MHz, CD_2Cl_2, δ ppm) δ_C δ 141.8 (C_7), 139.9 (C_2), 134.3 (C_4), 131.2 (C_6), 122.5 (C_3), 121.2 (C_5), 86.4 (C_1), 21.6 (C_8). MS-FAB: m/z 531.0, [Ru(η^6-benzene)-(**L2**)Cl]$^+$; 496.0, [Ru (η^6-benzene)(**L2**)]$^+$.

Crystallography. Crystals suitable for single-crystal X-ray analysis of compounds **1**, **2**, and **4** were selected and covered with Fomblin (polyfluoro ether oil) and mounted on a nylon loop. The data were collected at 110 K on a Bruker D8 Venture diffractometer equipped with a Photon II detector and an Oxford Cryosystem Cooler, using graphite-monochromated Mo Kα radiation (λ = 0.71073 Å). The data were processed using the APEX3 suite software package, which includes integration and scaling (SAINT), absorption corrections (SADABS),[32] and space group determination (XPREP). Structure solution and refinement were done using direct methods with the programs SHELXT 2014/5 and SHELXL (version 2018/3)[33] inbuilt in the APEX, SIR2019,[34] and WinGX-Version 2018.3[35] software packages. All non-hydrogen atoms were refined anisotropically. Hydrogen atoms were inserted in idealized positions and allowed to refine riding on the parent carbon or oxygen atom with C−H distances of 0.95, 0.98, 0.99, and 1.00 Å for aromatic, methyl, methylene, and methine H atoms, respectively. The molecular diagrams were drawn with ORTEP-3 (version 2014.1),[35] included in the software package. The data were deposited with the CCDC under deposit numbers 2062604 for **1**, 2062605 for **2**, and 2062606 for **4**.

Biological Assays. *Compound Stability in Biological Culture Medium.* Before assessment of the biological activity of compounds in cells, it is important to evaluate the compound stability in the cell culture medium. With that consideration, powdered compounds **1**−**4** were solubilized in DMSO and immediately after diluted in DMEM (Dulbecco's modified Eagle's medium) without phenol red (Invitrogen Corp., Grand Island, NY, USA) at a final concentration of 100 μM (assuring that the final concentration of DMSO does not exceed 0.1% v/v). The UV−visible spectrum of each compound was measured using a quartz cuvette with 1 cm path length in a wavelength range from 230 to 800 nm. Spectra were measured at 0 h and after 24 h and 48 h incubation at 37 °C in DMEM. The spectrum of each compound in DMSO at time 0 h was also acquired.

Cell Culture. Human colorectal carcinoma (HCT116) and normal dermal fibroblast cell lines were grown in DMEM (Invitrogen Corp., Grand Island, NY, USA) supplemented with 10% (v/v) fetal bovine serum and 1% (v/v) antibiotic/antimycotic solution (Invitrogen Corp.). A human colorectal carcinoma resistant to doxorubicin (HCT116dox) cell line was previously developed in the group[36] by exposing HCT116 sensitive cells to increasing concentrations of doxorubicin (Merck, Kenilworth, NJ, USA) for more than 40 passages (Figure S25). HCT116dox cells were grown under the same conditions as for HCT116 and fibroblasts but in the presence of 3.6 μM of doxorubicin to maintain resistance. The human ovarian carcinoma (A2780) cell line was cultivated using RPMI (Roswell Park Memorial Institute) medium supplemented with DMEM. Cells were grown in an incubator with a humidified atmosphere at 5% (v/v) CO_2 and 37 °C. All cell lines with the exception of HCT116dox were purchased from the ATCC.

Cellular Viability. Cells were plated in 96-well plates at 7.5 × 10^4 cells/mL and incubated at 37 °C with 5% (v/v) CO_2 for 24 h. After the 24 h period, the culture medium was replaced with a fresh medium containing 0.1−50 μM of compound **1**, **2**, **3**, **4**, **L1**, or **L2** and incubated for 48 h, as described previously.[37] Compounds and ligands to be used in cell-based assays were freshly prepared in DMSO and then immediately diluted in the respective culture medium, assuring a final percentage of 0.1% (v/v) of DMSO in the medium (no cytotoxicity to cells). DMSO 0.1% (v/v) was used as the vehicle control for normalization of the viability data for all cell lines.

Doxorubicin and cisplatin were used as positive controls (common chemotherapeutic agents), using DMSO and NaCl 0.9% (w/v) as vehicle controls, respectively. Cellular viability was evaluated using a CellTiter 96Aqueous Non-Radioactive Cell Proliferation Assay (Promega, Madison, WI, USA) with 3-(4,5-dimethylthiazol-2-yl)-5-(3-carboxymethoxyphenyl)-2-(4-sulfophenyl)-2*H*-tetrazolium, inner salt (MTS), as previously described.[37] In metabolically active cells, enzymes present in the mitochondria catalyze a reaction in which NADPH/NADH is produced. These enzyme compounds reduce the MTS reagent into a brownish product called formazan, which can be quantified by measuring the absorbance at 490 nm. The quantity of product produced is directly proportional to the number of viable cells in the culture. The amount of formazan product formed was measured with a Biorad Model 680 microplate reader (Bio-Rad, Hercules, CA, USA). The relative half-maximum inhibitory concentration (relative IC_{50}) was calculated using GraphPad Prism 6. (GraphPadSoftware, La Jolla, CA, USA). The selectivity index (SI) was calculated for A2780 by dividing the IC_{50} value of fibroblasts by the IC_{50} value of A2780 for each compound.

Evaluation of Apoptosis. Apoptosis in A2780 cells was evaluated using the Dead Cell Apoptosis Kit with Annexin V-FITC/PI (fluorescein isothiocyanate; propidium iodide) (Thermo Fisher Scientific) as previously described.[38] Cells were plated in 6-well plates at 1 × 10^5 cells/mL and remained in the incubator for 24 h. The medium was removed and a fresh medium added containing the IC_{50} value of compound **1**, **3**, DMSO 0.1% (v/v) (vehicle control), 3.5 μM cisplatin (positive control), or NaCl 0.001% (p/v) (vehicle control of cisplatin). After 48 h the cells were collected with trypsin, washed with PBS 1x and incubated with Annexin V-FITC buffer 1x, Annexin V-FITC, and 100 μg/mL of PI at 37 °C for 15 min at room temperature. The probes used have distinct fluorescence excitation and emission wavelengths, allowing the quantification of cells in the various phases of apoptosis and necrosis.

Cells were then analyzed in an Attune acoustic focusing cytometer (Thermo Fisher Scientific, Waltham, MA, USA), and data were used as inputs to the corresponding software Attune Cytometric Software v2.1 (Thermo Fisher Scientific).

Western Blot fox BAX and BCL-2 Quantification. A2780 cells were seeded on 25 cm^2 t-flasks with a cell density of 7.5 × 10^5 cells and incubated for 24 h. The medium was replaced by fresh medium containing the IC_{50} of the compound **1**, **3**, 0.4 μM doxorubicin (positive control), or DMSO 0.1% (v/v) (vehicle control) and incubated for 48 h. Cells were washed and collected using 1x PBS and a cell scraper and resuspended in lysis buffer. The following procedure was similar to previously reported,[39] with the exception that a PVDF membrane was used (GE Healthcare) and the signal was acquired

https://doi.org/10.1021/acs.inorgchem.1c00527
Inorg. Chem. 2021, 60, 8011−8026

using a Hyperfilm ECL apparatus (Gthat E Healthcare). The analysis was performed using FIJI software. The percentage of BAX and BCL-2 was calculated relative to the normalized β-actin values and to the value of the sample containing DMSO.

Mitochondrial Membrane Potential. The mitochondrial membrane potential was assessed using a JC-1 dye (Abnova Corporation, Walnut, CA, USA) according to the manufacturer's instructions. Cells were plated in 6-well plates at 1×10^5 cells/mL and incubated for 24 h. The medium was removed and replaced by fresh medium containing DMSO 0.1% (v/v) (vehicle control), The IC_{50} concentration of compound **1**, **3**, 3.5 μM cisplatin (positive control), or NaCl 0.001% (w/v) (vehicle control of cisplatin). After 48 h of incubation cells were collected, washed with PBS 1x, and incubated with the JC-1 probe for 20 min. Cells were then collected and resuspended in PBS 1x. When the membrane is intact, the probe enters mitochondria, where it accumulates emitting red fluorescence, whereas when there is an increase in mitochondrial membrane permeability the probe can enter but to a lesser degree, not reaching sufficient concentration to form aggregates and therefore remaining in its monomeric form emitting green fluorescence.[40] Cell analysis was performed with an Attune Acoustic Focusing Flow Cytometer (ThermoFisher Scientific, Waltham, MA, USA).

Evaluation of Autophagy. Autophagy in A2780 cells was evaluated using the Autophagy Assay Kit (Abcam, Cambridge, U.K.) according to the manufacturer's instructions. Cells were plated at 1×10^5 cells/mL in 6-well plates and incubated. After 24 h the medium was replaced with a fresh medium with 0.1% (v/v) DMSO (vehicle control), 1.5 μM rapamycin (positive control), and the IC_{50} concentration of compound **1**, **3**, 3.5 μM cisplatin (positive control), or NaCl 0.001% (w/v) (vehicle control of cisplatin). After 48 h cells were detached from the wells using trypsin and washed with Assay Buffer 1x. Afterward cells were incubated for 30 min in RPMI culture medium with Green Stain solution and 5% FBS. Then cells were collected and washed with Assay Buffer 1x and resuspended in Assay Buffer 1x afterward. The detection reagent becomes brightly fluorescent in vesicles produced during autophagy, allowing the quantification of autophagic cells. Cell analysis was performed with an Attune Acoustic Focusing Flow Cytometer (ThermoFisher Scientific, Waltham, MA, USA).

Evaluation of the Production of Reactive Oxygen Species (ROS). A2780 cells were plated at 1×10^5 cells/mL in 6-well plates and incubated for 24 h. The medium was replaced with a fresh medium containing 0.1% (v/v) DMSO (vehicle control), 25 μM hydrogen peroxide (positive control), IC_{50} concentration of compound **1**, **3**, 3.5 μM cisplatin (positive control), or NaCl 0.001% (w/v) (vehicle control of cisplatin) and incubated for 48 h. Cells were then collected with trypsin, washed with PBS 1x, and incubated with 10 μM of 2′,7′-dichlorodihydrofluorescein diacetate (H_2DCF-DA) (ThermoFisher Scientific, Waltham, MA, USA) for 20 min. This method allows the relative quantification of ROS production because after H_2DCF-DA internalizes and it is in the presence of ROS, intracellular esterases will remove the acetate groups of H_2DCF-DA, therefore increasing its fluorescence.[41] Cells were analyzed with an Attune Acoustic Focusing Flow Cytometer (ThermoFisher Scientific, Waltham, MA, USA).

***Ex Ovo* CAM Assay.** Fertilized eggs were incubated at 37 °C and 90% (v/v) relative humidity. After 72 h, they were gently opened into weighing boats, ensuring that the yolk sack blood vessels were facing upward, and then covered with a similar but punctured weighing boat. Subsequently, the eggs were incubated for 24 h for them to stabilize. Afterward, three silicone O-rings were placed above the blood vessels of each embryo, and in the area delimited by each O-ring 40 μL of either 0.1% (v/v) DMSO in PBS 1x (vehicle control) or the IC_{50} concentration in A2780 of compound **1** or **3** were added. Images of the O-ring interior were captured using a digital USB Microscope Camera (Opti-Tekscope OT-V1) immediately after exposure (0 h) and after 24 and 48 h of incubation at 37 °C and 90% (v/v) relative humidity. Image analysis was performed using FIJI software as previously described.[42] The percentage of newly formed vessels was calculated relative to the 0 h time point and to the number of newly formed vessels in the vehicle control.

Interaction with pDNA. Plasmid DNA was obtained from *E. coli* transformed cells grown overnight in LB liquid medium (Applichem, Darmstadt, Germany) with 100 μg mL^{-1} Ampicilin (Bioline, London, U.K.) at 37 °C with stirring. DNA extraction was performed using an Invisorb Spin Plasmid Mini Two Kit (Invitek, Berlin, Germany) according to the manufacturer's instructions. A 100 ng portion of pUC18 was incubated with increasing concentrations of complex **1** or **3** for 24 and 48 h at 37 °C in reaction buffer (5 mM Tris-HCl, 50 mM NaCl pH 7.02). Cells treated with 0.1% (v/v) DMSO were used as a vehicle control. Untreated plasmid and linearized plasmid DNA (with *Hin*dIII endonuclease) were incubated under the same conditions. Electrophoresis was performed at 80 V constant voltage for 1 h in 1x TAE buffer, and the gel was analyzed with a Gel Doc EZ Imager (Bio-Rad).

Cell Migration Assay. Fibroblasts were seeded in 35 mm^2 tissue plates and grown at 37 °C, 5% (v/v) CO_2, and 99% (v/v) relative humidity until a confluent monolayer was obtained. Using a sterile 200 μL micropipette tip, a scratch was made on the surface of the tissue culture plate. The cells were then exposed to 0.1% (v/v) DMSO (vehicle control) or the IC_{50} concentration of compound **1** or **3**. Cells were photographed using a digital USB Microscope Camera (Opti-Tekscope OT-V1) immediately after exposure (0 h) and after 24 h of incubation at 37 °C, 5% (v/v) CO_2, and 99% (v/v) relative humidity. Afterward the scratches were measured using ImageJ software and the regeneration percentage was calculated.[43]

Cell Cycle. A2780 cells were plated at 3×10^5 cells/mL in 6-well plates and incubated for 8 h. To achieve cell synchronization, a double thymidine block was performed as described previously.[8] Cells were incubated with fresh medium containing 2 mM thymidine for 16 h (first block) followed by an incubation for 8 h with fresh medium without thymidine. For the second block, cells were incubated with fresh medium containing 2 mM thymidine for 16 h. After this, cells were exposed to 0.1% (v/v) DMSO (vehicle control), 0.4 μM doxorubicin (positive control), or the IC_{50} concentration of compound **1** or **3** and incubated. Cells were collected with trypsin after 0, 5, 24, and 32 h of incubation and washed with PBS 1x. Cells were resuspended in PBS, and 1 mL of cold 80% (v/v) ethanol solution was added carefully. Samples were incubated for a minimum of 16 h at 4 °C, and ethanol was removed after centrifugation followed by an incubation with RNase (50 μg/mL) for 30 min. Propidium iodide was then added to a final concentration of 25 μg/mL. Cells were analyzed with an Attune Acoustic Focusing Flow Cytometer (ThermoFisher Scientific, Waltham, MA, USA).

Statistical Analysis. All data are expressed as mean ± SEM from two independent experiments. The statistical significance was evaluated using Student's t test. When $p < 0.05$, the results were considered statistically significant.

***In Vivo* Toxicity Assessment Using Zebrafish Embryos.** Zebrafish embryo experiments were carried out in less than 5 days. At this early stage of development (0−5 days post fertilization (dpf)), zebrafish embryos are not defined as protected and, therefore, do not fall within the regulatory frameworks related to animal experimentation defined by the European directive Directive 2010/63/EU on the protection of animals used for scientific purposes.[44]

The wild type zebrafish were housed in a water recirculation system under controlled physicochemical conditions of temperature, pH, and conductivity of 26 ± 2 °C, 7−7.5, and 400−600 μS/cm, respectively.[45] Adult fish were fed brine shrimp once a day and twice with Gemma Micro 300 (skretting). The fertilized eggs were collected after natural spawning and housed in Petri dishes until their use. The embryos were exposed to ruthenium complexes as soon as possible after fertilization was confirmed by visual inspection. Then, toxicological analyzes were carried out on the basis of the approved standard OECD TG 236: Fish Embryo Toxicity Test (FET),[46] with modifications. For the study, 4 replicates of 12 embryos were distributed for each of the five concentrations tested for compounds **1**−**4**. The compounds were dissolved in water containing 1% DMSO. When the results of some preliminary tests were taken into account,

https://doi.org/10.1021/acs.inorgchem.1c00527
Inorg. Chem. 2021, 60, 8011−8026

Scheme 3. Synthesis of Ru(II) Compounds 1−4

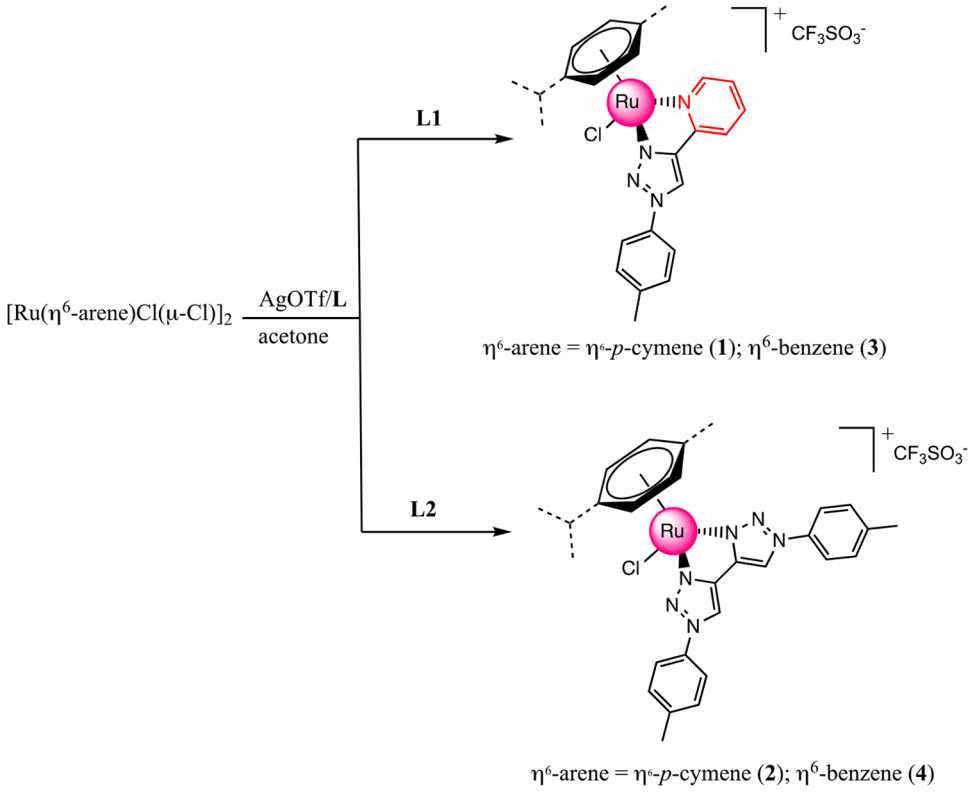

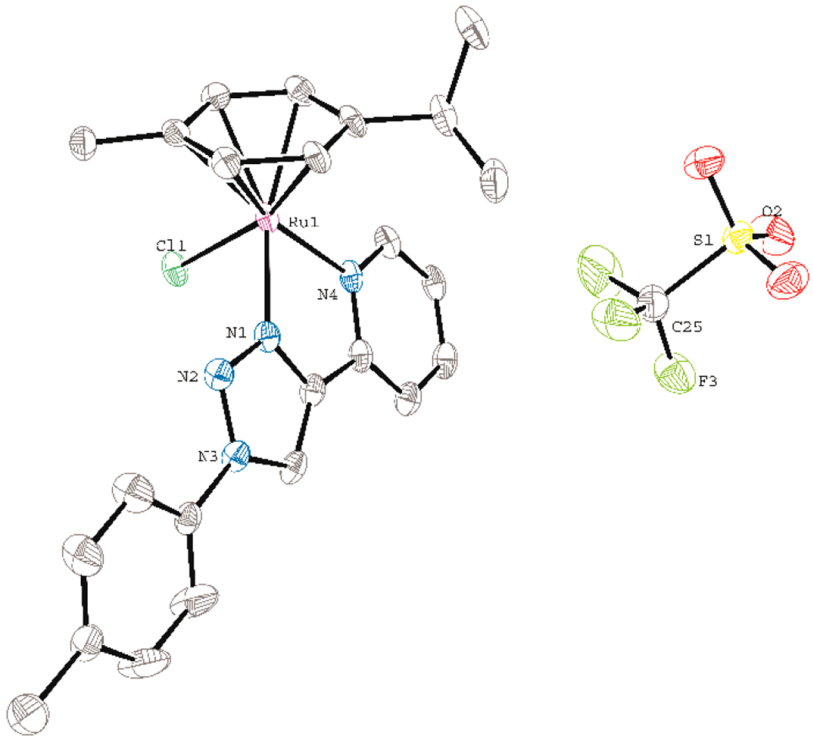

Figure 1. ORTEP-3 diagram of compound **1**, using 50% probability level ellipsoids. All hydrogen atoms are omitted for clarity. Selected bond lengths (Å): Ru1−N1 2.054(3), Ru1−N4 2.131(2), Ru1−Cl1 2.3844(8), Ru1−C15 2.208(3), Ru1−C16 2.176(3), Ru1−C17 2.195(3), Ru1−C18 2.187(3), Ru1−C19 2.199(3), Ru1−C20 2.203(3). Selected bond angles (deg): N1−Ru1−N4 76.15(10), N1−Ru1−Cl1 83.21(7), N4−Ru1−Cl1 83.54(7).

the concentrations analyzed for **1** were 1, 10, 20, 30, and 40 μM, those for **2** were 1, 5, 10, 15, and 20 μM), those for **3** were 0.5, 1, 5, 10, and 15 μM, and those for **4** were 0.1, 1, 10, 30, and 50 μM. All experiments and protocols were approved by the animal care and use committee of the University of Santiago de Compostela and the standard protocols of Spain (CEEA-LU-003 and Directive 2012-63-

https://doi.org/10.1021/acs.inorgchem.1c00527
Inorg. Chem. 2021, 60, 8011−8026

EU). The toxicity evaluation data were analyzed by probit analysis using ToxRat software (ToxRat Solutions, 2003, ToxRat Software for statistical analysis of bioassays, Alsdorf, Germany).

RESULTS AND DISCUSSION

Synthesis and Characterization. The synthesis of 1,2,3-triazoles **L1** and **L2** used in this work was performed by following the procedures reported in the literature.[30,31] Compounds **1**−**4** were synthesized by the reaction of the appropriate ruthenium arene dimer $[(\eta^6\text{-arene})Ru(\mu\text{-}Cl)Cl]_2$[7] (arene = benzene or *p*-cymene) with 1 equiv of $AgCF_3SO_3$ in the presence of the corresponding 1,2,3-triazole ligand **L1** or **L2** (Scheme 3).

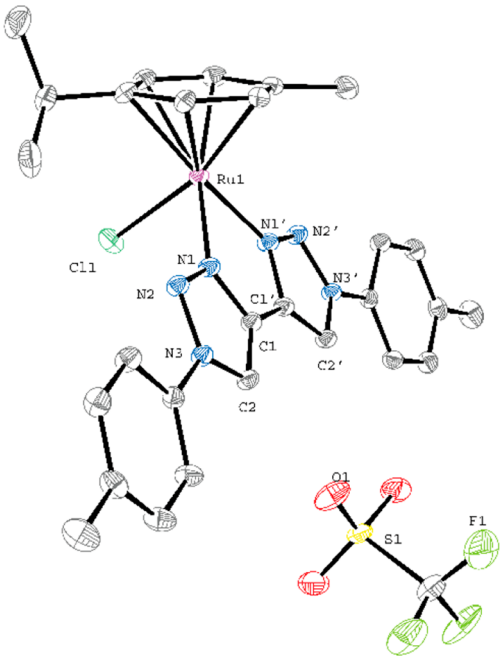

Figure 2. ORTEP-3 diagram of compound **2**, using 50% probability level ellipsoids. All hydrogen atoms and a molecule of cocrystallized dichloromethane are omitted for clarity. Selected bond lengths (Å): Ru1−N1 2.0907(15), Ru1−N1′ 2.0986(15), Ru1−Cl1 2.3921(5), Ru1−C10 2.1912(18), Ru1−C11 2.1659(18), Ru1−C12 2.1861(19), Ru1−C13 2.1921(18), Ru1−C14 2.1897(19), Ru1−C15 2.1736(19). Selected bond angles (deg): N1−Ru1−N1′ 75.50(6), N1−Ru1−Cl1 86.30(4), N4−Ru1−Cl1 84.06(5).

All of the synthesized compounds were characterized by means of IR and ^1H and ^{13}C NMR spectroscopy, mass spectrometry, and elemental analysis. The NMR spectra were consistent with the proposed structures. The ^1H NMR spectrum of **1** suggests a loss of the 2-fold symmetry of the *p*-cymene arene ligand upon coordination, displaying four doublets at 5.70, 5.74, 5.90, and 5.94 ppm. In contrast, the ^1H NMR spectrum of **2** shows two doublets at 5.67 and 5.92 ppm, reflecting the symmetry of compound **2**. **3** and **4** both display a singlet resonance at 6.64 and 6.07 ppm, respectively, for the protons of the benzene ring in their ^1H NMR spectra. Apart from the arene resonances, the ^1H NMR spectra of **1**−**4** show the characteristic signal of the triazole ligands **L1** and **L2** shifted downfield in comparison to the free ligand. In addition, the mass spectra of complexes **1**−**4** showed the expected $[Ru(p\text{-cymene})(L)Cl]^+$ and $[Ru(benzene)(L)Cl]^+$ peaks as the most abundant ions.

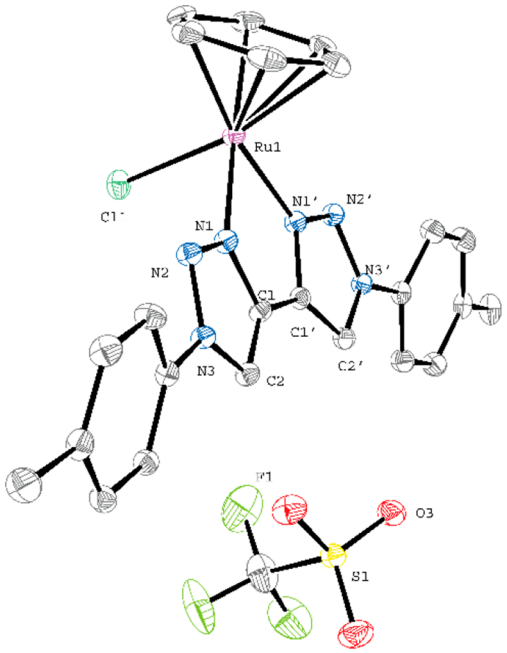

Figure 3. ORTEP-3 diagram of compound **4**, using 50% probability level ellipsoids. All hydrogen atoms are omitted for clarity. Selected bond lengths (Å): Ru1−N1 2.0821(17), Ru1−N1′ 2.0744(17), Ru1−Cl1 2.3922(5), Ru1−C10 2.159(2), Ru1−C11 2.186(2), Ru1−C12 2.165(2), Ru1−C13 2.184(2), Ru1−C14 2.175(2), Ru1−C15 2.186(2). Selected bond angles: N1−Ru1−N1′ 74.80(6), N1−Ru1−Cl1 85.86(5), N4−Ru1−Cl1 86.61(5).

Single crystals of **1**, **2**, and **4** suitable for X-ray diffraction studies were obtained by slow diffusion of hexane into saturated solutions of dichloromethane. Single crystals of **3** could not be obtained. The crystal structures of **1**, **2**, and **4** are depicted in Figures 1−3, respectively, with their respective ORTEP diagrams and the most relevant bond distances and angles reported in the corresponding caption.

All three complexes show a half-sandwich three-legged piano-stool geometry around the Ru(II) metal center, with a *p*-cymene or benzene ligand in a η^6 coordination mode, an *N*,*N*′-triazole-pyridine or *N*,*N*′-bis-triazole chelating ligand, and a chlorine atom bound to the metal center. In these complexes, the Ru1−Cl1 and the Ru−C(η^6-arene) bond distances have comparable values. In **1**, the Ru1−N1(triazole) bond distance is slightly shorter than those reported for analogous compounds by Sarkar et al.[47] and Elliot et al. and shorter than those observed in complexes **2** and **4**.[48,49] An analysis of the supramolecular arrangement in **1** shows the existence of weak intermolecular $\pi-\pi$ stacking interactions between the rings of the *p*-cymene ligand and the *p*-tolyl substituent of the *N*,*N*′-chelating ligand, as well as other intra- and intermolecular nonclassical C−H···N, C−H···O and C−H. . .Cl hydrogen bonds. In **2** and **4**, the solid-state arrangement involving the cation and anion is defined by nonclassical hydrogen bonds between the triazole C−H and the oxygen atoms of the triflate anion and shows evidence of favorable intermolecular $\pi-\pi$ stacking interactions between a triazole ring and a *p*-tolyl ring of a symmetry-related adjacent molecule and also nonclassical C−H···Cl hydrogen bonds.

Stability of Compounds 1−4 in Culture Medium. The stability of the compounds in DMEM culture medium was evaluated to gain insights into their possible application in the biological assays. For this analysis, powdered compounds **1**−**4**

https://doi.org/10.1021/acs.inorgchem.1c00527
Inorg. Chem. 2021, 60, 8011−8026

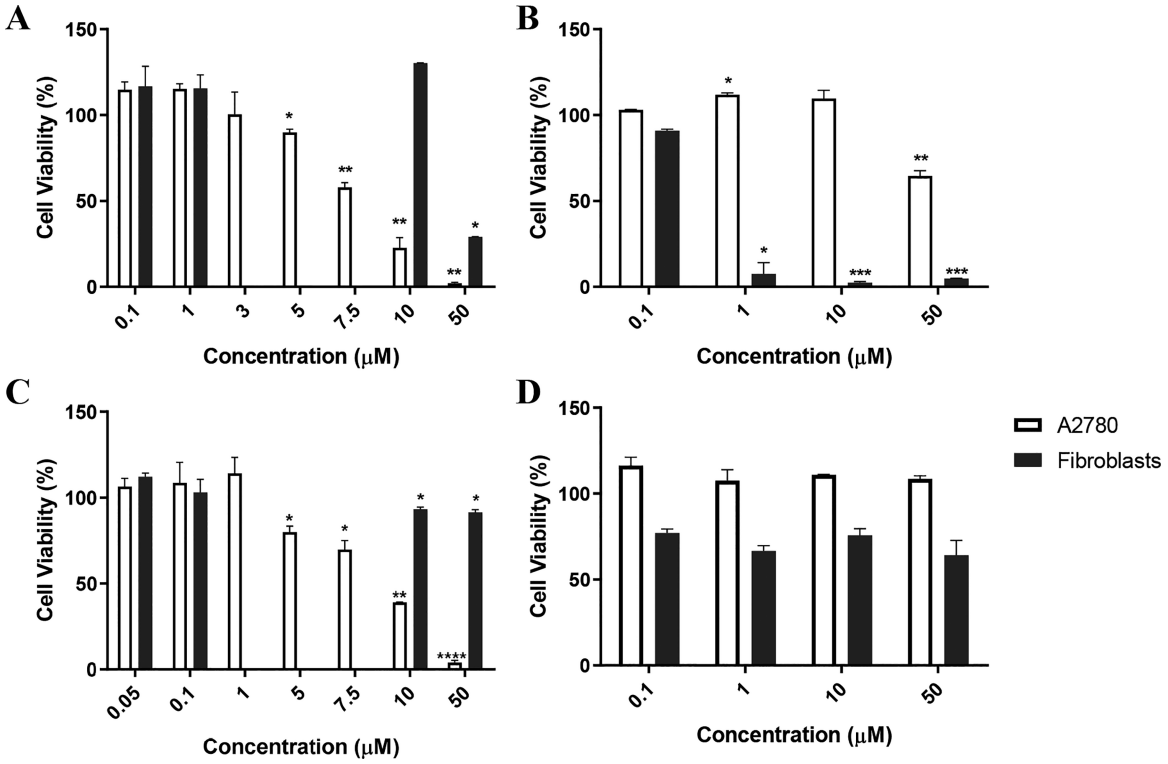

Figure 4. Antiproliferative effect in A2780 colorectal carcinoma cell line (white bars) and in normal dermal fibroblasts (black bars) after 48 h exposure to increasing concentrations of compounds (A) **1**, (B) **2**, (C) **3**, and (D) **4**. The cell viability percentage was determined by the MTS method. Data were normalized to DMSO 0.1% (v/v) vehicle control and expressed as mean ± SEM of three independent assays. The symbols * and **** indicate that the Student's *t* test *p* values are <0.01 and <0.005, respectively, in comparison to control conditions.

Table 1. Relative IC_{50} Values (μM) Obtained for Compounds 1−4 and for Ligands L1 and L2 in Human Cancer Cell Lines and in Normal Human Fibroblasts

	IC_{50} (μM)				
	A2780	HCT116	HCT116dox	fibroblast	SI
1	7.6 ± 0.03	12.1 ± 0.01	>50	44.2 ± 0.01	5.8
2	47.6 ± 0.01	>50	>50	0.50 ± 0.03	0.01
3	7.26 ± 0.05	>50	>50	>50	6.9
4	>50	>50	>50	>50	
L1	35.1 ± 0.5	40.8 ± 0.6	17.6 ± 0.3	>50	nd
L2	>50	>50	>50	>50	nd
cisplatin[a]	1.9 ± 0.2	nd	nd	nd	nd
Dox[a]	nd	0.5 ± 0.1	>6	nd	nd

[a]Relative IC_{50} values for cisplatin and doxorubicin (Dox) are calculated using the same experimental conditions as those used for **1**−**4**. nd denotes not determined.

were first solubilized in DMSO and then in DMEM, assuring that no more than 0.1% (v/v) of the solvent was present in the cell culture solution. An analysis of Figure S26 shows the existence of two absorption peaks located at 240−260 and 280−310 nm in all compounds that prevail throughout te time after incubation at 37 °C in DMEM, suggesting that compounds **1**−**4** preserve their structure in this media. Nevertheless, for compounds **2** and **4** a decrease in the absorbance values is observed with time, indicating a decreased solubility (Figure S26). No significant solubility issues were observed for compounds **1** and **3** (Figure S26). The spectra of compounds in DMSO seems to resemble the spectra of the compounds in DMEM (Figure S26). However, due to the high absorption of DMSO at 230−250 nm, it was not possible to detect the peak of the compounds at 240−260 nm. Overall, despite the loss of solubility of compounds **2** and **4** with time, the absence of changes in compound peaks suggests that we can further evaluate their biological activity in DMEM. Complexes were first dissolved in DMSO prior to dilution in DMEM (assuring that no more than 0.1% (v/v) DMSO was present in the media) and freshly used in all biological analyses.

Cytotoxic Potential. The effect of Ru(II) compounds **1**−**4** and the respective ligands **L1** and **L2** on the viability of two tumor cell lines (A2780 and HCT116) and in normal primary dermal fibroblasts was evaluated using the MTS assay (Figure 4 and Figures S27 and S28). The cytotoxicity was evaluated through concentration response graphics obtained by treating the cancer and normal cell lines with different concentrations of compounds for 48 h at 37 °C (Figure 4 and Figures S27 and S28), and expressed as the relative half-maximum inhibitory concentration, IC_{50} (concentration where 50% of the cell

https://doi.org/10.1021/acs.inorgchem.1c00527
Inorg. Chem. 2021, 60, 8011−8026

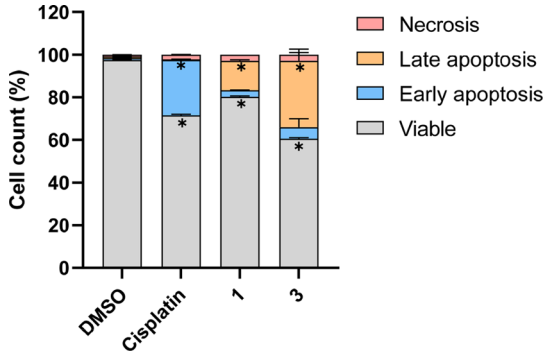

Figure 5. Apoptosis induction in A2780 cells after 48 h exposure to the IC_{50} concentration of **1** or **3** evaluated by flow cytometry. DMSO 0.1% (v/v) was the vehicle control, and cisplatin (IC_{50} of 3.5 μM) was used as a positive control. Data are expressed as mean ± SEM of three independent assays. *, p value <0.05 relative to the vehicle control sample. Data from flow cytometry are presented in Figure S30.

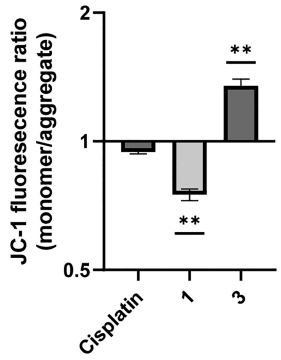

Figure 7. JC-1 monomer/aggregate fluorescence ratio in A2780 cells after 48 h exposure to the IC_{50} concentration of **1** or **3**, 3.5 μM cisplatin (positive control), or DMSO 0.1% (v/v) evaluated by flow cytometry. Data were normalized to the DMSO 0.1% (v/v) control. (**, p value <0.05).

growth is inhibited) (Table 1). In addition, to get insights into the efficacy of these compounds against colorectal cancer cells resistant to chemotherapeutic agents commonly used in the clinics, we have also examined the antiproliferative effect of the compounds in a doxorubicin-resistant HCT116 cell line previously described by our group[36] and obtained by exposing sensitive HCT116 cells to increasing concentrations of doxorubicin until a stable phenotype was obtained (more than 40 passages; Figure S25). This cell line is resistant for concentrations up to 6 μM (Table 1). Interestingly, this cell line reproduces a patient's acquired resistance in the way that the underlying mechanism of resistance is the overexpression of P-glycoprotein (P-gp).[36]

As observed in Figure 4, Figure S27, and Table 1, no antiproliferative effect was observed after the incubation of all cell lines with compound **4**. Compound **2** showed a high antiproliferative effect in normal fibroblasts but no effect in the viability of tumor cells (SI value of 0.01 with respect to A2780). Interestingly, compounds **1** and **3**, both bearing the mixed triazole-pyridine **L1**, exhibited considerable antiproliferative effects in the A2780 cell line (IC_{50} values of 7.6 and 7.26 μM, respectively) with almost no effects on normal fibroblasts (IC_{50} values of 44.2 and >50 μM, respectively). Indeed, the SI values are 5.8 and 6.9 for **1** and **3**, respectively. On consideration of A2780 cells, the antiproliferative effect is in the order **3** ≈ **1** > **2** > **4**. Compound **1** also demonstrated a good antiproliferative activity in the colorectal carcinoma cell

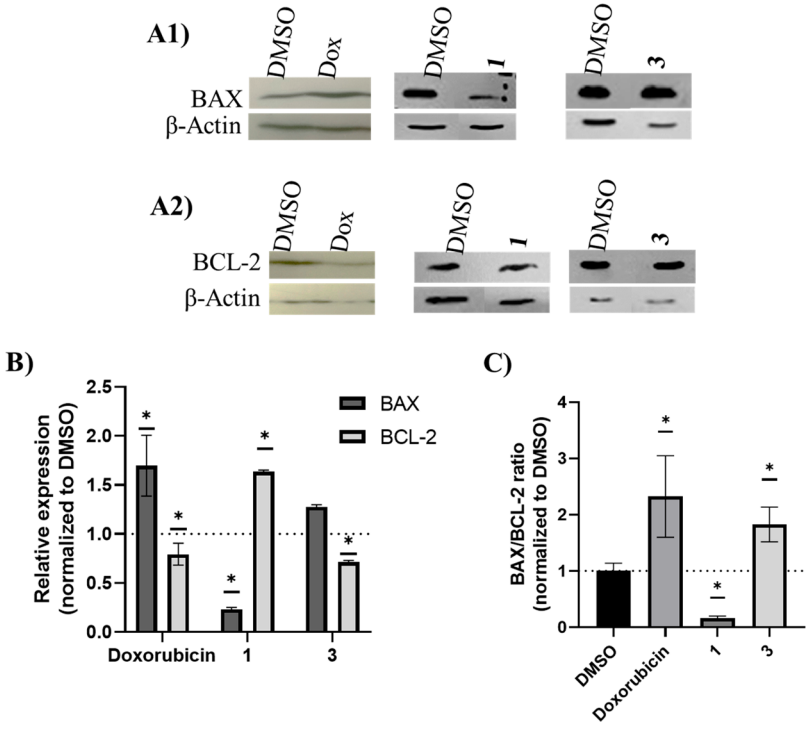

Figure 6. Expression of BAX and BCL-2 proteins in in A2780 cells after 48 h exposure to the IC_{50} concentration of **1** or **3**, 0.12 μM Doxorubicin (Dox), or DMSO 0.1% (v/v). (A) Western blot images for quantification of (A1) BAX and (A2) BCl-2. (B) BAX (dark gray) and BCL-2 (light gray) relative protein expression after normalization against β-actin and the respective control (0.1% (v/v) DMSO). The control value of **1** is represented as a dotted line in the graphic. (C) BAX/BCL-2 ratio of A2780 cells. (*, p value <0.05 relative to the control sample).

https://doi.org/10.1021/acs.inorgchem.1c00527
Inorg. Chem. 2021, 60, 8011−8026

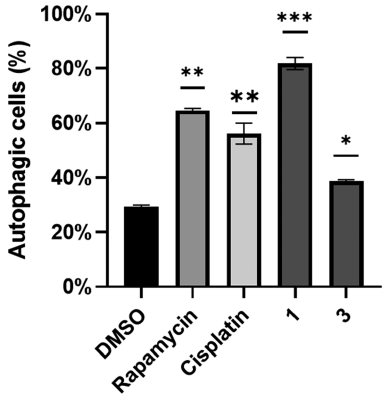

Figure 8. Induction of autophagy after exposure of A2780 cells to the IC_{50} concentration of compound **1** or **3** for 48 h. A 0.1% (v/v) DMSO solution was used as the vehicle control and 3.5 μM cisplatin and 1.5 μM rapamycin were used as positive controls. (**, p value <0.05; ***, p value <0.001).

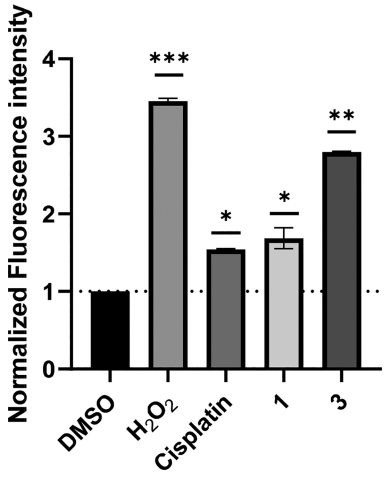

Figure 9. Reactive oxygen species (ROS) induced in A2780 cells after 48 h of exposure to the IC_{50} concentration of compound **1** or **3**. A 0.1% (v/v) DMSO solution was used as the vehicle control, and 3.5 μM cisplatin and 25 μM H_2O_2 were used as positive controls. Values were normalized to the control, represented as a dotted line (*, p value <0.05; **, p value <0.001; ***, p value <0.0005).

line (HCT116) with an IC_{50} value of 12.1 μM but had no effect on HCT116dox, suggesting that this complex is not a suitable antiproliferative agent toward multidrug-resistant cells (Figure S27 and Table 1). Indeed, when we observe Figure S27, it is possible to see that none of the compounds are effective toward the HCT116dox resistant cell line (Table 1). Interestingly, ligand **L1** presented a higher cytotoxic effect in the HCT116dox resistant cell line in comparison to the dox-sensitive cell line (Table 1 and Figures S27 and S28). This effect was reversed when **L1** was complexed with Ru to form compound **1**, with a higher IC_{50} value in HCT116dox in comparison to that for the HCT116 cell line (Table 1 and Figure S27).

Notwithstanding that the relative IC_{50} values for **1** and **3** are higher than those exhibited by cisplatin (1.9 ± 0.2 μM in A2780) and doxorubicin (0.5 ± 0.1 μM in HCT116) (Figure S29), they both display IC_{50} values in a low micromolar range (<10 μM) in the A2780 cell line. This values are lower than those displayed by the related ruthenium compound [Ru(η^6-benzene)(bpy)Cl][PF_6], bearing bipyridine as an N^N chelating ligand, which was inactive against A2780 cell line,[50] and comparable to the values of other Ru(II) N^N chelating pyridine derivatives.[8,19,51]

Despite the moderate to low antiproliferative effect of ligand **L1** and the absence of effect of ligand **L2** (Figure S28 and Table 1), our results demonstrate that the N^N chelating ligand (**L1** or **L2**) in arene Ru complexes plays a significant role in the cytotoxic activity of these compounds, while the presence of a different arene fragment (benzene or *p*-cymene) does not affect their anticancer activity. Indeed, the presence of **L1**, a N^N mixed triazole-pyridine ligand, in **1** and **3** leads to higher antiproliferative effects in comparison to **2** and **4** (with **L2**, a N^N ditriazole ligand), which correlates with the cytotoxicity order **L1** > **L2** (Figure S28 and Table 1). In fact, **L2** substitution results in no cytotoxic activity, as shown by the IC_{50} values of compounds **2** and **4** (Table 1) in tumor cell lines. Despite the fact that we cannot exclude that the low cytotoxicity in tumor cell lines of compounds **2** and **4** might be correlated to their loss of solubility in DMEM (Figure S26), it is of note the compound **2** has a very high cytotoxicity in normal dermal fibroblasts at 48 h (Figure S28 and Table 1), removing it from further analysis. The reduction of cell viability promoted by **1** and **3** in A2780 cells and the absence of cytotoxicity toward human dermal cells encouraged us to further explore the mechanisms involved in their antiproliferative effects. Since both **1** and **3** showed higher activity against A2780, all subsequent experiments were carried out with this cell line.

Cell Death Mechanism. *Apoptosis Assay.* In order to gain insight into whether the reduction in cell viability is arising from apoptosis, induction of apoptosis was analyzed by Annexin V-FITC/PI double staining of the A2780 cell line which was exposed to the IC_{50} concentration of compound **1** or **3**. PI dye binds to cells with a compromised membrane, thus staining cells in necrosis and in late apoptosis. On the other hand, Annexin V-FITC binds to a phospholipid component (phosphatidylserine) of the cell membrane that in early apoptosis becomes exposed on the cell surface.[52] Cells were analyzed by flow cytometry (Figure S30), and the results are shown in Figure 5.

The results depicted in Figure 5 show that both compounds can induce apoptosis. Indeed, compounds **1** and **3** induced apoptosis in approximately 17% and 37% of A2780 cells. No necrosis seems to be induced by these compounds (Figure 5). To further confirm the induction of apoptosis by both compounds, BAX and BCL2 protein levels, a proapoptotic and an antiapoptotic protein, respectively, were analyzed by Western blot. An increased expression of antiapoptotic protein BCL2 determines cell survival (ratio BAX/BCL2 < 1), and intrinsic apoptosis is triggered by the increased expression of proapoptotic proteins, such as BAX (ratio BAX/BCL2 > 1).[53] Expression levels of BAX and BCL-2 were evaluated in A2780 cells exposed to the IC_{50} concentration of compound **1** or **3** or to 0.12 μM doxorubicin (positive control) for 48 h (Figure 6). β-Actin levels were used as a control for protein loading, and 0.1% (v/v) DMSO was used as a vehicle control. The BAX/BCL-2 ratios are shown in Figure 6.

Figure 6 shows that A2780 cells exposed to **3** present a BAX/BCL-2 ratio 1.8× higher than that of control cells, while cells exposed to **1** have a ratio 7.7× lower than that of DMSO-treated cells. These results indicate that, in fact, BAX-mediated mitochondrial apoptosis might be triggered when A2780 cells are exposed to **3**. The permeabilization of the mitochondrial

https://doi.org/10.1021/acs.inorgchem.1c00527
Inorg. Chem. 2021, 60, 8011−8026

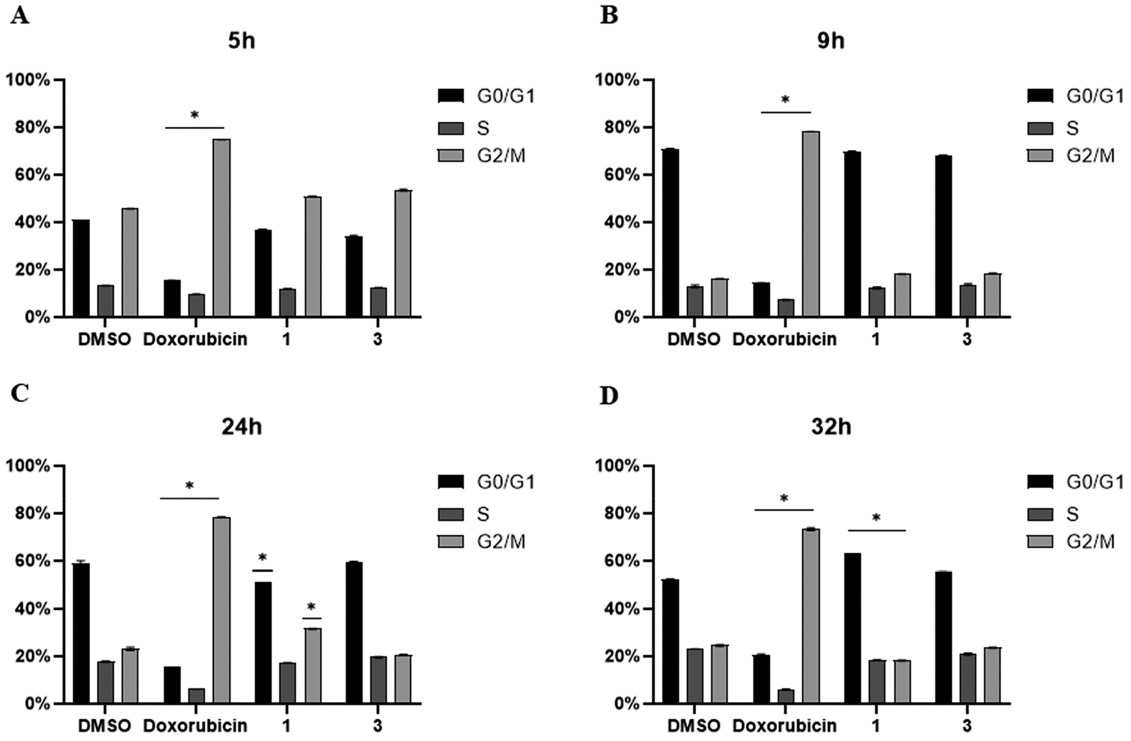

Figure 10. Cell cycle progression analysis on the A2780 cell line after exposure to the IC_{50} concentration of compound **1** or **3** for 5 h (A), 9 h (B), 24 h (C), or 32 h (D). A 0.1% (v/v) DMSO was used as a vehicle control, and 0.4 μM doxorubicin was used as a positive control (*, p value <0.05 relative to control).

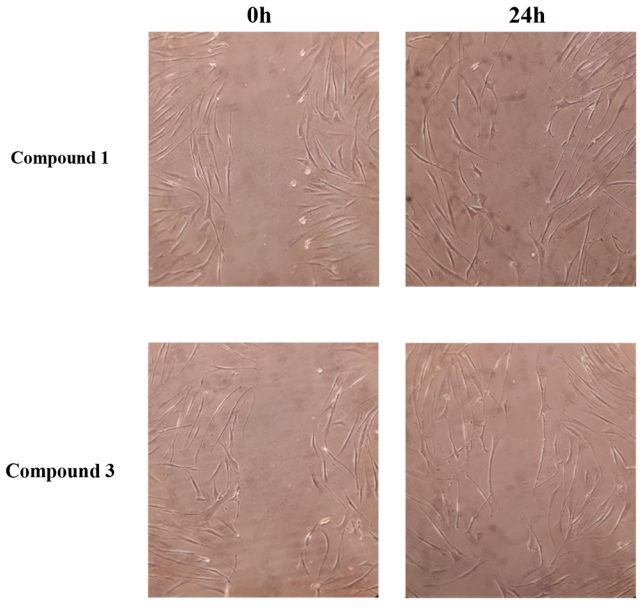

Figure 11. Representative images of the wound-healing assay of normal fibroblasts at 0 and 24 h.

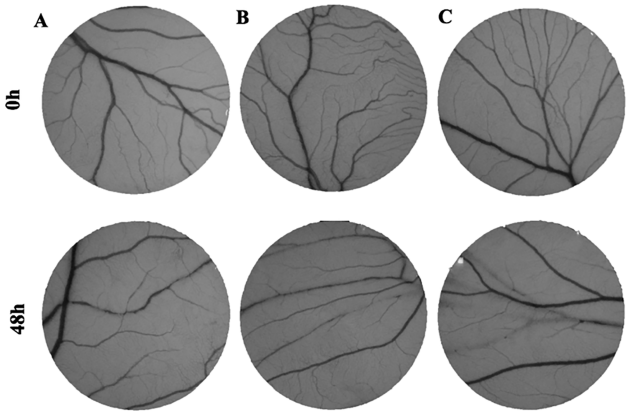

Figure 12. Examples of CAM area 0 and 48 h after exposure to (A) phosphate buffer saline (PBS, control), (B) compound **1**, and (C) compound **3**.

membrane that is achieved by pore formation due to the entry of proapoptotic proteins (such as BAX) in the mitochondrial membrane leads to the release of cytochrome *c* from the mitochondria to the cytoplasm, a crucial step for the activation of the intrinsic apoptotic pathway.[54] On consideration of this, the mitochondrial membrane potential was analyzed to confirm that compound **3** induces an intrinsic apoptosis.

A2780 cells were exposed to an IC_{50} concentration of compound **1** or **3** for 48 h and stained with JC-1 dye, which stays in its monomer form when the mitochondrial membrane permeability is compromised and aggregates when there is no variation of membrane potential.[48] A 0.1% (v/v) DMSO solution was used as the vehicle control. Cells were analyzed by flow cytometry, and the results are shown in Figure 7.

Figure 7 shows that exposure of A2780 cells to compound **3** increased mitochondrial membrane permeability, while exposure to compound **1** did not. These findings confirm the results from Figure 6 indicating that compound **3** triggers an intrinsic apoptosis pathway and suggesting that compound **1** may trigger apoptosis through an extrinsic pathway. However, the results from Figures 5 and 6 agree that apoptosis do not seem to be the main cell death mechanism underlying compound **1** loss of cell viability in A2780 cells. on

https://doi.org/10.1021/acs.inorgchem.1c00527
Inorg. Chem. 2021, 60, 8011−8026

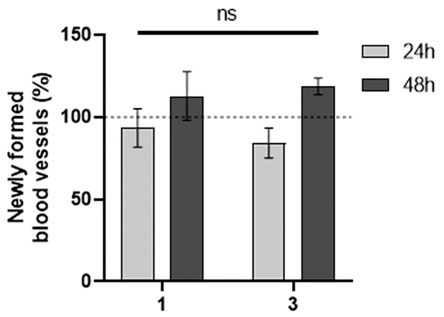

Figure 13. Newly formed arterioles obtained 24 and 48 h after exposure to **1** or **3**. Values were normalized to the number of tertiary veins obtained after exposure to control (PBS) and to the number of tertiary veins obtained in the corresponding CAM area at 0 h incubation in the same embryo. The dotted line at 100% refers to the PBS sample. The concentration of compounds used was equal to the IC_{50} value. Error bars represent the standard deviation from the mean of six independent eggs.

consideration of these results, autophagic cell death was assessed.

Autophagy Assay. A2780 cells were exposed to an IC_{50} concentration of compound **1** or **3** for 48 h, and the induction of autophagy was analyzed by staining cells with a dye that labels autophagosomes and autophagolysosomes. A 0.1% (v/v) DMSO solution, 3.5 μM cisplatin, and 1.5 μM rapamycin were used as a vehicle control and positive controls, respectively. Cells were analyzed by flow cytometry, and the results are shown in Figure 8.

As observed in Figure 8, compound **1** can induce autophagic death in 80% of A2780 cells, which is 2.7× higher in comparison to control and higher in comparison to the rapamycin positive control. On the other hand, exposure to compound **3** led to an induction of autophagy in only 40% of the cells, which represents a 1.3× increase in comparison to the control (Figure 8). These results indicate that autophagy may be the main cell death mechanism resulting from exposure to **1**, while in the case of compound **3**, the reduction of cell viability may be due to the triggering of both autophagy and apoptosis (Figures 8 and 5, respectively).

There is some evidence that Ru(II) compounds including Ru^{II}(*p*-cymene) are able to induce apoptosis and/or autophagy of cancer cells.[9,55,56] Reactive oxygen species (ROS) are critical for regulating the balance between autophagy and apoptosis in cancer cells upon different drug treatments.[57] Considering this, we have analyzed the induction of ROS by both compounds.

Reactive Oxygen Species (ROS). The exposure of A2780 cancer cells to the IC_{50} concentrations of both compounds **1** and **3** for 48 h led to an increase in intracellular ROS (Figure 9). To measure ROS, a 2′,7′-dichlorodihydrofluorescein diacetate (H2DCF-DA) dye was used, which in the presence of peroxides is rapidly oxidized to 2′,7′-dichlorofluorescein (DCF), becoming highly fluorescent. The fluorescence is proportional to the amount of ROS inside cells.A 0.1% (v/v) DMSO solution and 3.5 μM cisplatin and 25 μM hydrogen peroxide (H_2O_2) were used as vehicle and positive controls, respectively. Cells were analyzed by flow cytometry, and the results are shown in Figure 9.

Figure 9 shows an increased fluorescence of A2780 cells treated with both compounds. Indeed, cells treated with compound **1** or **3** showed 1.7× or 2.8× more intracellular ROS in comparison to control cells (Figure 9). These results suggest that the exposure of A2780 cells to both compounds leads to an increase in oxidative stress (ROS generation) that triggers autophagic cell death in the case of compound **1** (Figure 8) and both autophagy and apoptosis to cope with the high levels of ROS in the case of compound **3** (Figures 5 and 8). There is unequivocal preclinical and clinical evidence that ROS influence the genotoxic stress caused by chemotherapeutic

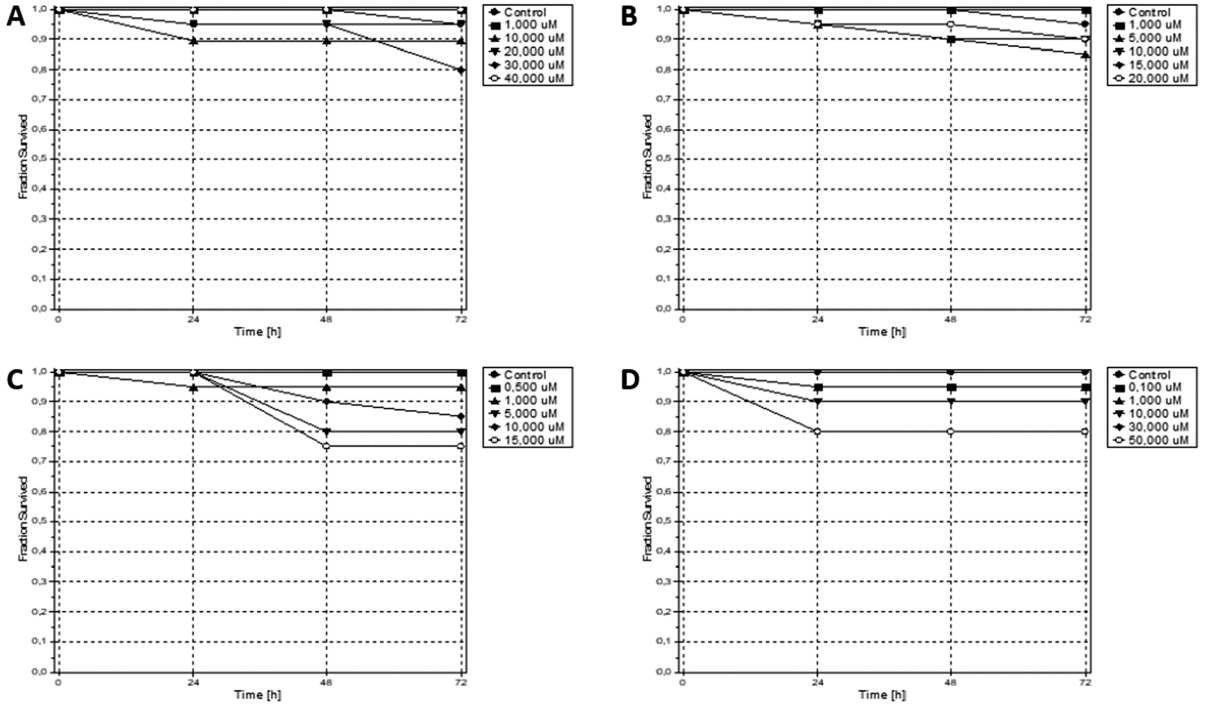

Figure 14. Cumulative mortality over (72 h) for complex **1** (A), complex **2** (B), complex **3** (C), and complex **4** (D).

https://doi.org/10.1021/acs.inorgchem.1c00527
Inorg. Chem. 2021, 60, 8011−8026

agents.[58] ROS can induce DNA damage and affect the DNA damage response, triggering cell death. Moreover, DNA is a target for several Ru(II) compounds.[9] To get evidence of DNA as a direct target of compounds **1** and **3**, we next studied their *in vitro* interaction with plasmidic DNA (pDNA).

***In Vitro* Interaction with Plasmidic DNA.** To address this issue, pDNA was incubated with increasing concentrations of compound **1** or **3** during 48 and 72 h (Figure S31). Figure S31 shows that compounds **1** and **3** do not induce pDNA cleavage. An increase in concentration and incubation time for both compounds does not lead to significant changes in the pDNA isoforms in terms of DNA cleavage or pattern of migration in the gel. These results suggest that both compounds do not show the ability to induce DNA damage by cleavage or alter its in-gel mobility.

Cell Cycle Assay. Previously, Ru(II) complexes have been described as prompting ROS induction, which promoted cell cycle arrest in S and G0/G1 phases in cancer cells.[59,60] Considering that, we further studied the effect of compounds **1** and **3** in A2780 cell cycle progression by quantifying the DNA content at different stages of the cell cycle using a PI as a dye. A2780 cells were exposed to the IC_{50} concentration of compound **1** or **3** for 5, 9, 24, and 32 h after being synchronized with a double thymidine block. A 0.1% (v/v) DMSO solution and 0.4 μM doxorubicin were used as a vehicle control and positive control, respectively. Cells were analyzed by flow cytometry, and the results are shown in Figure 10.

Figure 10 shows that cells treated with doxorubicin became arrested in the G2/M phase after 5 h of exposure, while the other samples progressed through their cycle normally. At 24 h, a delay in G2/M phase with a decrease of cells in G0/G1 is observed for compound **1** (Figure 10). Between 24 and 32 h of exposure, there was an increase in cells in the G0/G1 phase in samples treated with compound **1**, suggesting that cells that were previously in G2/M progressed to G0/G1 but again delay their progression to S phase, indicating that this compound delays cell cycle progression (Figure 10). Cells treated with compound **3** progressed through the cell cycle similarly to control cells. These results indicate that compound **1** may have some cytostatic potential interfering with cell cycle progression and that compound **3** does not seem to interfere with cell cycle progression (Figure 10). Once again, we observe that despite **1** and **3** showing similar cytotoxicity (IC_{50}) values in A2780 cells (Table 1), the cellular mechanisms underlying the loss of viability (Figure 4) are different, with **1** inducing ROS that led to cell cycle delay and cell death via mostly autophagy, while **3** induces ROS but cell death was triggered via intrinsic apoptosis and also autophagy (Figures 5−10).

Cell Migration Assay. As cell migration and invasion are central in pathological and physiological phenomena, including cancer metastasis and wound healing, these processes can be explored as therapeutic targets.[61] The identification of compounds effective in avoiding cancer cell migration and invasion is of utmost importance to avoid metastization.[62] Previously, an arene Ru(II) complex (arene = benzene) has been described as a potent inhibitor against proliferation, migration, and invasion of breast cancer cells.[63] To understand if compounds **1** and **3** have an influence on cell migration, a scratch test was performed by exposing primary dermal fibroblasts to the IC_{50} concentrations of compounds **1** and **3** for 24 h. After 24 h, the scratch regeneration was evaluated for control cells and for cells exposed to **1** and **3**. Fibroblasts exposed to the vehicle control (0.1% DMSO) and to compound **3** showed a 46.3 ± 0.33% and 45.8 ± 2.85% of regeneration, respectively, while for fibroblasts treated with **1** a lower regeneration (30.6 ± 1.39%) was observed (Figure 11), suggesting that, likely the previous described arene Ru(II) complex, this compound inhibits cells capacity to migrate and might be important in a therapeutic context. In contrast, compound **3** does not affect cell migration.

Interestingly, recently a heterometallic ruthenium−gold complex was shown to display antiproliferative, antimigratory, and antiangiogenic properties in renal cancer.[64] These results prompted us to additionally study the antiangiogenic potential of both compounds **1** and **3**. Some years ago, the chick chorioallantoic membrane (CAM) model was described as an excellent *in vivo* model to study the effect of newly identified molecules in angiogenesis and tumor invasion of colorectal, prostate, brain cancer, and ovarian cancers.[65] Moreover, *in vivo* model toxicity effects might also be studied, as recently described by us for palladacycles.[66] This prompted us to also test compounds **1** and **3** in this model in terms of toxicity and antiangiogenic potential using as a model *ex ovo* CAM.[67]

***Ex Ovo* Chick Chorioallantoic Membrane (CAM) Assay.** Three O-rings were placed on the yolk sack of chicken embryos as described in the Experimental Section and for each O-ring, a different condition was added: PBS (control), compound **1**, and compound **3**. O-rings were photographed at 0, 24, and 48 h after the addition of the different conditions (Figure 12), and afterward the percentage of newly formed arterioles was calculated. The *in vivo* results show that compounds **1** and **3** do not influence the angiogenesis process significantly (Figure 13). It is worth noting that **1** and **3** did not induce death of the chicken embryos for the tested concentrations.

Zebrafish Model. Zebrafish is an animal model that in recent years has gained great relevance in various areas of research, due to the fact that it presents important advantages. Some of them are high fecundity, small size, rapid embryonic development, and optical transparency.[68,69] Furthermore, the zebrafish is very similar to mammals in most aspects of embryonic development and in the cardiovascular, somite, muscular, skeletal, and neuronal systems.[70] In addition, the zebrafish genome has approximately 70% homology with the human genome and 84% of the known genes are associated with human diseases.[71,72] These advantages make zebrafish a good model for studying the toxicity of new compounds. Thus, a fish embryo acute toxicity (FET) test was performed. For that, zebrafish embryos of 2−4 hpf were exposed to five different concentrations of all ruthenium compounds and every 24−72 h four lethal end points were analyzed: coagulated embryos, lack of somite formation, absence of tail shedding, and lack of heartbeat. As a result, none of the compounds showed signs of lethal toxicity in the embryos. In fact, at 72 h, a survival greater than 75% was observed in all cases (Figure 14), which is relevant in the case of complexes **1** and **3** due to their good cytotoxic activity in A2780 tumor cells linked to the low toxicity also demonstrated in the chicken embryo.

■ CONCLUSIONS

In this work, the four new Ru(II) compounds [Ru(η^6-arene)(L)Cl][CF_3SO_3] (arene = *p*-cymene, **L1** (**1**); arene = *p*-cymene, **L2** (**2**); arene = benzene, **L1** (**3**); arene = benzene, **L2** (**4**); **L1** = 2-[1-(*p*-tolyl)-1*H*-1,2,3-triazol-4-yl]pyridine; **L2** = 1,1′-di-*p*-tolyl-1*H*,1′H-4,4′-bi(1,2,3-triazole)) were prepared

https://doi.org/10.1021/acs.inorgchem.1c00527
Inorg. Chem. 2021, 60, 8011−8026

and fully characterized. The antiproliferative effect of complexes **1**−**4** was analyzed in different tumor and normal cell lines. While compounds **2** and **4** had no effect on the tumor cell lines, **1** and **3** were active against the A2780 cancer cell line with no cytotoxic effect on normal primary fibroblasts at the IC_{50} concentration of ovarian cancer cells. Interestingly, the antiproliferative activity correlated well with the type of chelating triazole ligand (**L1** or **L2**). The presence of **L1**, a mixed triazole-pyridine ligand, in the molecular composition of compounds **1** and **3** leads to higher antiproliferative effects in comparison to **2** and **4**, bearing the ditriazole ligand **L2**. Furthermore, compound **1** also exhibited cytotoxic activity toward the HCT116 colorectal cell line. Our results show that both **1** and **3** induce ROS, which triggers cell death via autophagy (compound **1**) or autophagy and apoptosis (compound **3**). These cell death mechanisms are the cause of the cell viability reduction observed. Compounds **1** and **3** did not have any effect on plasmid DNA fragmentation, and **1** was demonstrated to delay cell cycle progression and cell migration. Compound **1** induces some neovascularization after 24 h, while **3** shows reduced neovascularization capability. In overall, these results suggest that the mechanisms of cytotoxicity of compounds **1** and **3** render these compounds as promising new Ru(II) arene chemotherapeutic agents. As for NKP1339 currently in clinical trials, the complexes induce ROS production[12] and consequently promote cell death via autophagy (compounds **1** and **3**) or intrinsic apoptosis (compound **3**). The ability of compound **1** to delay cell cycle progression might also be correlated to damages induced by ROS, as shown for NKP1339.[12] Moreover, the lack of DNA fragmentation renders these compounds with an advantage over acquired resistance of cells to chemotherapeutic drugs, such as cisplatin, by activating mechanisms of DNA damage repair.[7] Importantly, the delay of cell migration promoted by **1** suggests that this compound might be useful in a tumor microenvironment context, by stabilizing the irregular leakiness characteristic of tumor vasculature and consequently promoting the compound distribution in the tumor, hence minimizing metastasis formation. Compounds **1** and **3** are not toxic, both *in vitro* (evaluated in normal human fibroblasts) and *in vivo* (evaluated in zebrafish and chicken embryos). Altogether, these results demonstrate the potential of these newly synthesized mixed triazole-pyridine-based ruthenium(II) compounds and, particularly, compound **1** for further *in vivo* mice xenograft studies to validate their antitumor potential.

■ ASSOCIATED CONTENT

Supporting Information

The Supporting Information is available free of charge at https://pubs.acs.org/doi/10.1021/acs.inorgchem.1c00527.

> Structural determination data, stability of complexes in cell culture medium, antiproliferative effect of complexes **1**−**4** and ligands **L1** and **L2**, cytotoxicity of cisplatin and doxorubicin in the A2780 cell line, flow cytometry results of the apoptosis assay in A2780 cells exposed to **1** and **3**, and a pUC18 fragmentation analysis (PDF)

Accession Codes

CCDC 2062604−2062606 contain the supplementary crystallographic data for this paper. These data can be obtained free of charge via www.ccdc.cam.ac.uk/data_request/cif, or by emailing data_request@ccdc.cam.ac.uk, or by contacting The Cambridge Crystallographic Data Centre, 12 Union Road, Cambridge CB2 1EZ, UK; fax: +44 1223 336033.

■ AUTHOR INFORMATION

Corresponding Authors

Oscar A. Lenis-Rojas − *Instituto de Tecnologia Química e Biológica António Xavier, ITQB NOVA, Universidade Nova de Lisboa, 2780-157 Oeiras, Portugal*; Email: oscar.rojas@itqb.unl.pt

Alexandra R. Fernandes − *UCIBIO, Departamento Ciências da Vida, Faculdade de Ciências e Tecnologia, Universidade Nova de Lisboa, 2829-516 Caparica, Portugal*; orcid.org/0000-0003-2054-4438; Email: ma.fernandes@fct.unl.pt

Beatriz Royo − *Instituto de Tecnologia Química e Biológica António Xavier, ITQB NOVA, Universidade Nova de Lisboa, 2780-157 Oeiras, Portugal*; orcid.org/0000-0002-7909-9992; Email: broyo@itqb.unl.pt

Authors

Rui Cabral − *UCIBIO, Departamento Ciências da Vida, Faculdade de Ciências e Tecnologia, Universidade Nova de Lisboa, 2829-516 Caparica, Portugal*

Beatriz Carvalho − *UCIBIO, Departamento Ciências da Vida, Faculdade de Ciências e Tecnologia, Universidade Nova de Lisboa, 2829-516 Caparica, Portugal*

Sofia Friães − *Instituto de Tecnologia Química e Biológica António Xavier, ITQB NOVA, Universidade Nova de Lisboa, 2780-157 Oeiras, Portugal*

Catarina Roma-Rodrigues − *UCIBIO, Departamento Ciências da Vida, Faculdade de Ciências e Tecnologia, Universidade Nova de Lisboa, 2829-516 Caparica, Portugal*

Jhonathan A. A. Fernández − *Laboratory of Zebrafish, Department of Medical Genetics and Genomic Medicine-School of Medical Sciences, University of Campinas (UNICAMP), Campinas 13083-887, Sao Paulo, Brazil; Departamento de Zoología Genética y Antropología Física, Facultad de Veterinaria, Universidad de Santiago de Compostela, 27002 Lugo, Spain*

Sabela F. Vila − *Departamento de Zoología Genética y Antropología Física, Facultad de Veterinaria, Universidad de Santiago de Compostela, 27002 Lugo, Spain*

Laura Sanchez − *Departamento de Zoología Genética y Antropología Física, Facultad de Veterinaria, Universidad de Santiago de Compostela, 27002 Lugo, Spain; Preclinical Animal Models Group, Health Research Institute of Santiago de Compostela (IDIS), A Coruña, Spain*

Clara S. B. Gomes − *LAQV-REQUIMTE UCIBIO, Departamento de Química, Faculdade de Ciências e Tecnologia, Universidade NOVA de Lisboa, 2829-516 Caparica, Portugal*; orcid.org/0000-0003-3672-0045

Complete contact information is available at: https://pubs.acs.org/10.1021/acs.inorgchem.1c00527

Funding

We are grateful to the Fundação da Ciência e a Tecnologia, FCT, fo rthe project MOSTMICRO-ITQB NOVA with references UIDB/04612/2020 and UIDP/04612/2020. The NMR spectrometers at CERMAX are integrated in the national NMR Network and partially supported through project 022162. We also thank the Analytic Services of ITQB and C. Almeida for elemental analysis and HRMS spectrometry. O.A.L.-R. acknowledges FCT, POPH-*Programa Operacional Potencial Humano*, and FSE (European Social

Fund) for the CEEC 2017 Initiative. Also, this work was supported by the Applied Molecular Biosciences Unit-UCIBIO which is financed by national funds from FCT (UIDP/04378/2020 and UIDB/04378/2020). J.A.A.F. acknowledges Coordenação de Aperfeiçoamento de Pessoal de Nível Superior-Brasil (CAPES) and the program CAPES/PRINT Proc. 88887.470075/2019−00. C.S.B.G. acknowledges the Associate Laboratory for Green Chemistry-LAQV, the Applied Molecular Biosciences Unit-UCIBIO (UIDB/50006/2020, UIDP/50006/2020, UIDB/04378/2020, UIDP/04378/2020), and X-ray infrastructure financed by FCT-MCTES through project RECI/BBB-BEP/0124/2012.

Notes

The authors declare no competing financial interest.

■ ACKNOWLEDGMENTS

We acknowledge I. Goncalves for preliminary pDNA and gDNA analysis and M. Baleia for BAX/BCL2 testing.

■ ABBREVIATIONS LIST

MS-FAB	fast atom bombardment mass spectroscopy
CT-DNA	calf thymus DNA
Tris	2-amino-2-(hydroxymethyl)propane-1,3-diol
MTS	3-(4,5-dimethylthiazol-2-yl)-5-(3-carboxymethoxyphenyl)-2-(4-sulfophenyl)-2*H*-tetrazolium, inner salt
H_2DCF-DA	2′,7′-dichlorodihydrofluorescein diacetate
hpf	hours postfertilization
FET	fish embryo acute toxicology test
PBS	phosphate-buffered saline

■ REFERENCES

(1) Sung, H.; Ferlay, J.; Siegel, R. L.; Laversanne, M.; Soerjomataram, I.; Jemal, A.; Bray, F. Global cancer statistics 2020: GLOBOCAN estimates of incidence and mortality worldwide for 36 cancers in 185 countries. *Ca-Cancer J. Clin.* **2021**, 209.

(2) Prager, G. W.; Braga, S.; Bystricky, B.; Qvortrup, C.; Criscitiello, C.; Esin, E.; Sonke, G. S.; Martínez, G. A.; Frenel, J. S.; Karamouzis, M.; Strijbos, M.; Yazici, O.; Bossi, P.; Banerjee, S.; Troiani, T.; Eniu, A.; Ciardiello, F.; Tabernero, J.; Zielinski, C. C.; Casali, P. G.; Cardoso, F.; Douillard, J. Y.; Jezdic, S.; McGregor, K.; Bricalli, G.; Vyas, M.; Ilbawi, A. Global Cancer Control: Responding to the Growing Burden, Rising Costs and Inequalities. *ESMO Open* **2018**, *3*, e000285.

(3) Abbas, Z.; Rehman, S. An Overview of Cancer Treatment Modalities. In *Neoplasm*; InTech: 2018.

(4) Dasari, S.; Tchounwou, P. B. Cisplatin in Cancer Therapy: Molecular Mechanisms of Action. *Eur. J. Pharmacol.* **2014**, *740*, 364−378.

(5) Ghosh, S. Cisplatin: The First Metal Based Anticancer Drug. *Bioorg. Chem.* **2019**, *88*, 102925−102945.

(6) Ndagi, U.; Mhlongo, N.; Soliman, M. Metal Complexes in Cancer Therapy - an Update from Drug Design Perspective. *Drug Des., Dev. Ther.* **2017**, *11*, 599−616.

(7) Chen, S. H.; Chang, J. Y. New Insights into Mechanisms of Cisplatin Resistance: From Tumor Cell to Microenvironment. *Int. J. Mol. Sci.* **2019**, *20*, 4136.

(8) Lenis-Rojas, O. A.; Robalo, M. P.; Tomaz, A. I.; Carvalho, A.; Fernandes, A. R.; Marques, F.; Folgueira, M.; Yáñez, J.; Vázquez-García, D.; López Torres, M.; Fernández, A.; Fernández, J. J. RuII(p-Cymene) Compounds as Effective and Selective Anticancer Candidates with No Toxicity in Vivo. *Inorg. Chem.* **2018**, *57*, 13150−13166.

(9) Lenis-Rojas, O. A.; Roma-Rodrigues, C.; Fernandes, A. R.; Marques, F.; Pérez-Fernández, D.; Guerra-Varela, J.; Sánchez, L.; Vázquez-García, D.; López-Torres, M.; Fernández, A.; Fernández, J. J. Dinuclear RuII(Bipy)$_2$ Derivatives: Structural, Biological, and in Vivo Zebrafish Toxicity Evaluation. *Inorg. Chem.* **2017**, *56*, 7127−7144.

(10) Lenis-Rojas, O. A.; Fernandes, A. R.; Roma-Rodrigues, C.; Baptista, P. V.; Marques, F.; Pérez-Fernández, D.; Guerra-Varela, J.; Sánchez, L.; Vázquez-García, D.; Torres, M. L.; Fernández, A.; Fernández, J. J. Heteroleptic Mononuclear Compounds of Ruthenium(II): Synthesis, Structural Analyses,: In Vitro Antitumor Activity and in Vivo Toxicity on Zebrafish Embryos. *Dalton Trans.* **2016**, *45*, 19127−19140.

(11) Lenis-Rojas, O. A.; Robalo, M. P.; Tomaz, A. I.; Fernandes, A. R.; Roma-Rodrigues, C.; Teixeira, R. G.; Marques, F.; Folgueira, M.; Yáñez, J.; Gonzalez, A. A.; Salamini-Montemurri, M.; Pech-Puch, D.; Vázquez-García, D.; Torres, M. L.; Fernández, A.; Fernández, J. J. Half-Sandwich Ru(p-Cymene) Compounds with Diphosphanes: In Vitro and in Vivo Evaluation as Potential Anticancer Metallodrugs. *Inorg. Chem.* **2021**, *60*, 2914−2930.

(12) Coverdale, J. P. C.; Laroiya-McCarron, T.; Romero-Canelón, I. Designing Ruthenium Anticancer Drugs: What Have We Learnt from the Key Drug Candidates? *Inorganics* **2019**, *7*, 31.

(13) Ang, W. H.; Daldini, E.; Scolaro, C.; Scopelliti, R.; Juillerat-Jeannerat, L.; Dyson, P. J. Development of organometallic ruthenium-arene anticancer drugs that resist hydrolysis. *Inorg. Chem.* **2006**, *45*, 9006−9013.

(14) Scolaro, C.; Bergamo, A.; Brescacin, L.; Delfino, R.; Cocchietto, M.; Laurenczy, G.; Geldbach, T. J.; Sava, G.; Dyson, P. J. In vitro and in vivo evaluation of ruthenium(II)-arene PTA complexes. *J. Med. Chem.* **2005**, *48*, 4161−4171.

(15) Berndsen, R. H.; Weiss, A.; Abdul, U. K.; Wong, T. J.; Meraldi, P.; Griffioen, A. W.; Dyson, P. J.; Nowak-Sliwinska, P. Combination of Ruthenium(II)-Arene Complex [Ru(H6-p-Cymene)Cl$_2$ (Pta)] (RAPTA-C) and the Epidermal Growth Factor Receptor Inhibitor Erlotinib Results in Efficient Angiostatic and Antitumor Activity. *Sci. Rep.* **2017**, *7*, 1−16.

(16) Adhireksan, Z.; Davey, G. E.; Campomanes, P.; Groessl, M.; Clavel, C. M.; Yu, H.; Nazarov, A. A.; Yeo, C. H.; Ang, W. H.; Droge, P.; Rothlisberger, U.; Dyson, P. J.; Davey, C. A. Ligand substitutions between ruthenium-cymene compounds can control protein versus DNA targeting and anticancer activity. *Nat. Commun.* **2014**, *5*, 3462−3475.

(17) Hayward, R. L.; Schornagel, Q. C.; Tente, R.; Macpherson, J. S.; Aird, R. E.; Guichard, S.; Habtemariam, A.; Sadler, P.; Jodrell, D. I. Investigation of the role of Bax, p21/Waf1 and p53 as determinants of cellular responses in HCT116 colorectal cancer cells exposed to the novel cytotoxic ruthenium(II) organometallic agent, RM175. *Cancer Chemother. Pharmacol.* **2005**, *55*, 577−583.

(18) Rilak Simović, A.; Masnikosa, R.; Bratsos, I.; Alessio, E. Chemistry and Reactivity of Ruthenium(II) Complexes: DNA/Protein Binding Mode and Anticancer Activity Are Related to the Complex Structure. *Coord. Chem. Rev.* **2019**, *398*, 113011.

(19) Morris, R. E.; Aird, R. E.; del Socorro Murdoch, P.; Chen, H.; Cummings, J.; Hughes, N. D.; Parsons, S.; Parkin, A.; Boyd, G.; Jodrell, D. I.; Sadler, P. J. Inhibition of Cancer Cell Growth by Ruthenium(II) Arene Complexes. *J. Med. Chem.* **2001**, *44*, 3616−3621.

(20) Aird, R. E.; Cummings, J.; Ritchie, A. A.; Muir, M.; Morris, R. E.; Chen, H.; Sadler, P. J.; Jodrell, D. I. In Vitro and in Vivo Activity and Cross Resistance Profiles of Novel Ruthenium (II) Organometallic Arene Complexes in Human Ovarian Cancer. *Br. J. Cancer* **2002**, *86*, 1652−1657.

(21) Chen, H.; Parkinson, J. A.; Morris, R. E.; Sadler, P. J. Highly Selective Binding of Organometallic Ruthenium Ethylenediamine Complexes to Nucleic Acids: Novel Recognition Mechanisms. *J. Am. Chem. Soc.* **2003**, *125*, 173−186.

(22) Chow, M. J.; Licona, C.; Pastorin, G.; Mellitzer, G.; Ang, W. H.; Gaiddon, C. Structural Tuning of Organoruthenium Compounds Allows Oxidative Switch to Control ER Stress Pathways and Bypass Multidrug Resistance. *Chem. Sci.* **2016**, *7*, 4117−4124.

https://doi.org/10.1021/acs.inorgchem.1c00527
Inorg. Chem. 2021, 60, 8011−8026

(23) Chow, M. J.; Babak, M. V.; Wong, D. Y. Q.; Pastorin, G.; Gaiddon, C.; Ang, W. H. Structural Determinants of P53-Independence in Anticancer Ruthenium-Arene Schiff-Base Complexes. *Mol. Pharmaceutics* **2016**, *13*, 2543−2554.
(24) Betanzos-Lara, S.; Salassa, L.; Habtemariam, A.; Sadler, P. J. Photocontrolled Nucleobase Binding to an Organometallic Ru(II) Arene Complex. *Chem. Commun.* **2009**, *43*, 6622−6624.
(25) Chen, Y.; Lei, W.; Hou, Y.; Li, C.; Jiang, G.; Zhang, B.; Zhou, Q.; Wang, X. Fine Control on the Photochemical and Photobiological Properties of Ru(II) Arene Complexes. *Dalton Trans.* **2015**, *44*, 7347−7354.
(26) Riedl, C. A.; Flocke, L. S.; Hejl, M.; Roller, A.; Klose, M. H. M.; Jakupec, M. A.; Kandioller, W.; Keppler, B. K. Introducing the 4-Phenyl-1,2,3-Triazole Moiety as a Versatile Scaffold for the Development of Cytotoxic Ruthenium(II) and Osmium(II) Arene Cyclometalates. *Inorg. Chem.* **2017**, *56*, 528−541.
(27) Riedl, C. A.; Hejl, M.; Klose, M. H. M.; Roller, A.; Jakupec, M. A.; Kandioller, W.; Keppler, B. K. N - And S -Donor Leaving Groups in Triazole-Based Ruthena(II)Cycles: Potent Anticancer Activity, Selective Activation, and Mode of Action Studies. *Dalton Trans.* **2018**, *47*, 4625−4638.
(28) Rono, C. K.; Chu, W. K.; Darkwa, J.; Meyer, D.; Makhubela, B. C. E. Triazolyl RuII, RhIII OsII, and IrIII Compounds as Potential Anticancer Agents: Synthesis, Structure Elucidation, Cytotoxicity, and DNA Model Interaction Studies. *Organometallics* **2019**, *38*, 3197−3211.
(29) Perrin, D. D.; Amarego, W.L.F.; Perrin, D.R. *Purification of Laboratory Chemicals*, 2nd ed.; Pergamon: 1980; pp 65−371.
(30) Bolje, A.; Urankar, D.; Košmrlj, J. Synthesis and NMR Analysis of 1,4-Disubstituted 1,2,3-Triazoles Tethered to Pyridine, Pyrimidine, and Pyrazine Rings. *Eur. J. Org. Chem.* **2014**, *2014*, 8167−8181.
(31) Hohloch, S.; Kaiser, S.; Duecker, F. L.; Bolje, A.; Maity, R.; Košmrlj, J.; Sarkar, B. Catalytic Oxygenation of Sp3 "C-H" Bonds with Ir(III) Complexes of Chelating Triazoles and Mesoionic Carbenes. *Dalton Trans.* **2015**, *44*, 686−693.
(32) Krause, L.; Herbst-Irmer, R.; Sheldrick, G. M.; Stalke, D. Comparison of Silver and Molybdenum Microfocus X-Ray Sources for Single-Crystal Structure Determination. *J. Appl. Crystallogr.* **2015**, *48*, 3−10.
(33) Sheldrick, G. M. Crystal Structure Refinement with SHELXL. *Acta Crystallogr., Sect. C: Struct. Chem.* **2015**, *71*, 3−8. (b) Hübschle, C. B.; Sheldrick, G. M.; Dittrich, B. ShelXle: A Qt Graphical User Interface for SHELXL. *J. Appl. Crystallogr.* **2011**, *44*, 1281−1284.
(34) Burla, M. C.; Caliandro, R.; Carrozzini, B.; Cascarano, G. L.; Cuocci, C.; Giacovazzo, C.; Mallamo, M.; Mazzone, A.; Polidori, G. Crystal Structure Determination and RefinementviaSIR2014. *J. Appl. Crystallogr.* **2015**, *48*, 306−309.
(35) Farrugia, L. J. WinGX and ORTEP for Windows: an update. *J. Appl. Crystallogr.* **2012**, *45*, 849−854.
(36) Pedrosa, P.; Mendes, R.; Cabral, R.; Martins, L.M.D.R.S.; Baptista, P. V.; Fernandes, A. R. Combination of chemotherapy and Au-nanoparticle photothermy in the visible light to tackle doxorubicin resistance in cancer cells. *Sci. Rep.* **2018**, *8*, 11429.
(37) Das, K.; Beyene, B. B.; Datta, A.; Garribba, E.; Roma-Rodrigues, C.; Silva, A.; Fernandes, A. R.; Hsiung Hung, C. EPR and electrochemical interpretation of bispyrazolylacetate anchored Ni(II) and Mn(II) complexes: cytotoxicity and anti-proliferative activity towards human cancer cell lines. *New J. Chem.* **2018**, *42*, 9126−9139.
(38) Ma, Z.; Zhang, B.; Guedes da Silva, M. F. C.; Silva, J.; Mendo, A. S.; Baptista, P. V.; Fernandes, A. R.; Pombeiro, A. J. L. Synthesis, Characterization, Thermal Properties and Antiproliferative Potential of Copper(II) 4'-Phenyl-Terpyridine Compounds. *Dalton Trans.* **2016**, *45*, 5339−5355.
(39) Almeida, J.; Roma-Rodrigues, C.; Mahmoud, A. G.; Guedes da Silva, M. F. C.; Pombeiro, A. J. L.; Martins, L. M. D. R. S.; Baptista, P. V.; Fernandes, A. R. Structural Characterization and Biological Properties of Silver(I) Tris(Pyrazolyl)Methane Sulfonate. *J. Inorg. Biochem.* **2019**, *199*, 110789.
(40) Sivandzade, F.; Bhalerao, A.; Cucullo, L. Analysis of the Mitochondrial Membrane Potential Using the Cationic JC-1 Dye as a Sensitive Fluorescent Probe. *Bio Protoc.* **2019**, *9*, 3128.
(41) Choroba, K.; Machura, B.; Raposo, L. R.; Małecki, J. G.; Kula, S.; Pająk, M.; Erfurt, K.; Maroń, A. M.; Fernandes, A. R. Platinum(Ii) Complexes Showing High Cytotoxicity toward A2780 Ovarian Carcinoma Cells. *Dalton Trans.* **2019**, *48*, 13081−13093.
(42) Roma-Rodrigues, C.; Heuer-Jungemann, A.; Fernandes, A. R.; Kanaras, A. G.; Baptista, P. V. Peptide-Coated Gold Nanoparticles for Modulation of Angiogenesis in Vivo. *Int. J. Nanomed.* **2016**, *11*, 2633−2639.
(43) Raposo, L. R.; Roma-Rodrigues, C.; Faísca, P.; Alves, M.; Henriques, J.; Carvalheiro, M. C.; Corvo, M. L.; Baptista, P. V.; Pombeiro, A. J.; Fernandes, A. R. Immortalization and Characterization of a New Canine Mammary Tumour Cell Line FR37-CMT: New Canine Mammary Tumour Cell Line FR37-CMT. *Vet. Comp. Oncol.* **2017**, *15*, 952−967.
(44) EU. Directive 2010/63/EU of the European parliament and of the council of 22 September 2010 on the protection of animals used for scientific purposes. *Off. J. EU* **2010**, *276*, 33−79.
(45) Westerfield, M. *The zebrafish book: A guide for the laboratory use of zebrafish (Danio rerio)*, 5th ed.; University of Oregon Press: 2007.
(46) Finney, D. J. *Probit Analysis*; Cambridge University Press: 1952.
(47) Hohloch, S.; Suntrup, L.; Sarkar, B. Arene-Ruthenium(II) and -Iridium(III) Complexes with "Click"-Based Pyridyl-Triazoles, Bis-Triazoles, and Chelating Abnormal Carbenes: Applications in Catalytic Transfer Hydrogenation of Nitrobenzene. *Organometallics* **2013**, *32*, 7376−7385.
(48) Scattergood, P. A.; Khushnood, U.; Tariq, A.; Cooke, D. J.; Rice, C. R.; Elliott, P. I. P. Photochemistry of $[Ru(Pytz)(Btz)_2]^{2+}$ and Characterization of a K1-Btz Ligand-Loss Intermediate. *Inorg. Chem.* **2016**, *55*, 7787−7796.
(49) Groom, C. R.; Bruno, I. J.; Lightfoot, M. P.; Ward, S. C. The Cambridge Structural Database. *Acta Crystallogr., Sect. B: Struct. Sci., Cryst. Eng. Mater.* **2016**, *72*, 171−179.
(50) Bugarcic, T.; Habtemariam, A.; Stepankova, J.; Heringova, P.; Kasparkova, J.; Deeth, R. J.; Johnstone, R. D. L.; Prescimone, A.; Parkin, A.; Parsons, S.; Brabec, V.; Sadler, P. J. The Contrasting Chemistry and Cancer Cell Cytotoxicity of Bipyridine and Bipyridinediol Ruthenium(II) Arene Complexes. *Inorg. Chem.* **2008**, *47*, 11470−11486.
(51) Romero-Canelón, I.; Salassa, L.; Sadler, P. J. The Contrasting Activity of Iodido versus Chlorido Ruthenium and Osmium Arene Azo- and Imino-Pyridine Anticancer Complexes: Control of Cell Selectivity, Cross-Resistance, P53 Dependence, and Apoptosis Pathway. *J. Med. Chem.* **2013**, *56*, 1291−1300.
(52) van Genderen, H. O.; Kenis, H.; Hofstra, L.; Narula, J.; Reutelingsperger, C. P. M. Extracellular Annexin A5: Functions of Phosphatidylserine-Binding and Two-Dimensional Crystallization. *Biochim. Biophys. Acta, Mol. Cell Res.* **2008**, *1783*, 953−963.
(53) Vicente, J. C.; Olay, S.; Lequerica-Fernandez, P.; Sanchez-Mayoral, J.; Junquera, L. M.; Fresno, M. F. Expression of Bcl-2 but Not Bax Has a Prognostic Significance in Tongue Carcinoma. *J. Oral Pathol. Med.* **2006**, *35*, 140−145.
(54) Loreto, C.; La Rocca, G.; Anzalone, R.; Caltabiano, R.; Vespasiani, G.; Castorina, S.; Ralph, D. J.; Cellek, S.; Musumeci, G.; Giunta, S.; Djinovic, R.; Basic, D.; Sansalone, S. The Role of Intrinsic Pathway in Apoptosis Activation and Progression in Peyronie's Disease. *BioMed Res. Int.* **2014**, *2014*, 1−10.
(55) Silva, S. L. R.; Baliza, I. R. S.; Dias, R. B.; Sales, C. B. S.; Rocha, C. A. G.; Soares, M. B. P.; Correa, R. S.; Batista, A. A.; Bezerra, D. P. Ru(II)-Thymine Complex Causes DNA Damage and Apoptotic Cell Death in Human Colon Carcinoma HCT116 Cells Mediated by JNK/P38/ERK1/2 via a P53-Independent Signaling. *Sci. Rep.* **2019**, *9*, 1−11.
(56) Lai, S.-H.; Li, W.; Wang, X.-Z.; Zhang, C.; Zeng, C.-C.; Tang, B.; Wan, D.; Liu, Y.-J. Apoptosis, Autophagy, Cell Cycle Arrest, Cell Invasion and BSA-Binding Studies in Vitro of Ruthenium(Ii) Polypyridyl Complexes. *RSC Adv.* **2016**, *6*, 63143−63155.

https://doi.org/10.1021/acs.inorgchem.1c00527
Inorg. Chem. 2021, 60, 8011−8026

(57) Gao, L.; Loveless, J.; Shay, C.; Teng, Y. Targeting ROS-Mediated Crosstalk between Autophagy and Apoptosis in Cancer. *Adv. Exp. Med. Biol.* **2020**, *1260*, 1−12.
(58) Srinivas, U. S.; Tan, B. W. Q.; Vellayappan, B. A.; Jeyasekharan, A. D. ROS and the DNA damage response in cancer. *Redox Biol.* **2019**, *25*, 101084.
(59) Han, B. J.; Jiang, G. B.; Wang, J.; Li, W.; Dai, Q. S.; Xie, Y. Y.; Lin, G. J.; Huang, H. L.; Liu, Y. J. Ruthenium(II) polypyridyl complexes: synthesis, cytotoxicity in vitro, reactive oxygen species, mitochondrial membrane potential and cell cycle arrest studies. *Transition Met. Chem.* **2015**, *40*, 153−160.
(60) Costa, M. S.; Gonçalves, Y. G.; Borges, B. C.; Silva, M. J. B.; Amstalden, M. K.; Costa, T. R.; Antunes, L. M. G.; Rodrigues, R. S.; Rodrigues, V. M.; Franca, E. F.; Zoia, M. A. P.; Araújo, T. G.; Goulart, L. R.; Poelhsitz, G. V.; Yoneyama, K. A. G. Ruthenium (II) complex cis-[RuII(η2-O2CC7H7O2)(dppm)2]PF6-hmxbato induces ROS-mediated apoptosis in lung tumor cells producing selective cytotoxicity. *Sci. Rep.* **2020**, *10*, 15410.
(61) Hulkower, K. I.; Herber, R. L. Cell Migration and Invasion Assays as Tools for Drug Discovery. *Pharmaceutics* **2011**, *3*, 107−124.
(62) Wang, X.; Decker, C. C.; Zechner, L.; Krstin, S.; Wink, M. In vitro wound healing of tumor cells: inhibition of cell migration by selected cytotoxic alkaloids. *BMC Pharmacol. Toxicol.* **2019**, *20*, 4.
(63) Wu, Q.; He, J.; Mei, W.; Zhang, Z.; Wu, X.; Sun, F. Arene ruthenium(ii) complex, a potent inhibitor against proliferation, migration and invasion of breast cancer cells, reduces stress fibers, focal adhesions and invadopodia. *Metallomics* **2014**, *6*, 2204−2212.
(64) Elie, B. T.; Pechenyy, Y.; Uddin, F.; Contel, M. A heterometallic ruthenium-gold complex displays antiproliferative, antimigratory, and antiangiogenic properties and inhibits metastasis and angiogenesis-associated proteases in renal cancer. *JBIC, J. Biol. Inorg. Chem.* **2018**, *23*, 399−411.
(65) Lokman, N. A.; Elder, A. S.; Ricciardelli, C.; Oehler, M. K. Chick chorioallantoic membrane (CAM) assay as an in vivo model to study the effect of newly identified molecules on ovarian cancer invasion and metastasis. *Int. J. Mol. Sci.* **2012**, *13*, 9959−9970.
(66) Reigosa-Chamorro, F.; Raposo, L. R.; Munín-Cruz, P.; Pereira, M. T.; Roma-Rodrigues, C.; Baptista, P. V.; Fernandes, A. R.; Vila, J. M. In Vitro and In Vivo Effect of Palladacycles: Targeting A2780 Ovarian Carcinoma Cells and Modulation of Angiogenesis. *Inorg. Chem.* **2021**, *60*, 3939−3951.
(67) Roma-Rodrigues, C.; Fernandes, A. R.; Baptista, P. V. Counteracting the Effect of Leukemia Exosomes by Antiangiogenic Gold Nanoparticles. *Int. J. Nanomed.* **2019**, *14*, 6843−6854.
(68) Olivares, C. I.; Field, J. A.; Simonich, M.; Tanguay, R. L.; Sierra-Alvarez, R. Arsenic (III, V), Indium (III), and Gallium (III) Toxicity to Zebrafish Embryos Using a High-Throughput Multi-Endpoint in Vivo Developmental and Behavioral Assay. *Chemosphere* **2016**, *148*, 361−368.
(69) Truong, L.; Harper, S. L.; Tanguay, R. L. Evaluation of Embryotoxicity Using the Zebrafish Model. *Methods Mol. Biol.* **2011**, *691*, 271−279.
(70) McCollum, C. W.; Ducharme, N. A.; Bondesson, M.; Gustafsson, J.-A. Developmental Toxicity Screening in Zebrafish. *Birth Defects Res., Part C* **2011**, *93*, 67−114.
(71) Gunnarsson, L.; Jauhiainen, A.; Kristiansson, E.; Nerman, O.; Larsson, D. G. J. Evolutionary Conservation of Human Drug Targets in Organisms Used for Environmental Risk Assessments. *Environ. Sci. Technol.* **2008**, *42*, 5807−5813.
(72) Howe, K.; Clark, M. D.; Torroja, C. F.; Torrance, J.; Berthelot, C.; Muffato, M.; Collins, J. E.; Humphray, S.; McLaren, K.; Matthews, L.; McLaren, S.; Sealy, I.; Caccamo, M.; Churcher, C.; Scott, C.; Barrett, J. C.; Koch, R.; Rauch, G.-J.; White, S.; Chow, W.; Kilian, B.; Quintais, L. T.; Guerra-Assunção, J. A.; Zhou, Y.; Gu, Y.; Yen, J.; Vogel, J.-H.; Eyre, T.; Redmond, S.; Banerjee, R.; Chi, J.; Fu, B.; Langley, E.; Maguire, S. F.; Laird, G. K.; Lloyd, D.; Kenyon, E.; Donaldson, S.; Sehra, H.; Almeida-King, J.; Loveland, J.; Trevanion, S.; Jones, M.; Quail, M.; Willey, D.; Hunt, A.; Burton, J.; Sims, S.; McLay, K.; Plumb, B.; Davis, J.; Clee, C.; Oliver, K.; Clark, R.; Riddle, C.; Elliott, D.; Threadgold, G.; Harden, G.; Ware, D.; Begum, S.; Mortimore, B.; Kerry, G.; Heath, P.; Phillimore, B.; Tracey, A.; Corby, N.; Dunn, M.; Johnson, C.; Wood, J.; Clark, S.; Pelan, S.; Griffiths, G.; Smith, M.; Glithero, R.; Howden, P.; Barker, N.; Lloyd, C.; Stevens, C.; Harley, J.; Holt, K.; Panagiotidis, G.; Lovell, J.; Beasley, H.; Henderson, C.; Gordon, D.; Auger, K.; Wright, D.; Collins, J.; Raisen, C.; Dyer, L.; Leung, K.; Robertson, L.; Ambridge, K.; Leongamornlert, D.; McGuire, S.; Gilderthorp, R.; Griffiths, C.; Manthravadi, D.; Nichol, S.; Barker, G.; Whitehead, S.; Kay, M.; Brown, J.; Murnane, C.; Gray, E.; Humphries, M.; Sycamore, N.; Barker, D.; Saunders, D.; Wallis, J.; Babbage, A.; Hammond, S.; Mashreghi-Mohammadi, M.; Barr, L.; Martin, S.; Wray, P.; Ellington, A.; Matthews, N.; Ellwood, M.; Woodmansey, R.; Clark, G.; Cooper, J. D.; Tromans, A.; Grafham, D.; Skuce, C.; Pandian, R.; Andrews, R.; Harrison, E.; Kimberley, A.; Garnett, J.; Fosker, N.; Hall, R.; Garner, P.; Kelly, D.; Bird, C.; Palmer, S.; Gehring, I.; Berger, A.; Dooley, C. M.; Ersan-Ürün, Z.; Eser, C.; Geiger, H.; Geisler, M.; Karotki, L.; Kirn, A.; Konantz, J.; Konantz, M.; Oberländer, M.; Rudolph-Geiger, S.; Teucke, M.; Lanz, C.; Raddatz, G.; Osoegawa, K.; Zhu, B.; Rapp, A.; Widaa, S.; Langford, C.; Yang, F.; Schuster, S. C.; Carter, N. P.; Harrow, J.; Ning, Z.; Herrero, J.; Searle, S. M. J.; Enright, A.; Geisler, R.; Plasterk, R. H. A.; Lee, C.; Westerfield, M.; de Jong, P. J.; Zon, L. I.; Postlethwait, J. H.; Nüsslein-Volhard, C.; Hubbard, T. J. P.; Crollius, H. R.; Rogers, J.; Stemple, D. L. The Zebrafish Reference Genome Sequence and Its Relationship to the Human Genome. *Nature* **2013**, *496*, 498−503.

https://doi.org/10.1021/acs.inorgchem.1c00527
Inorg. Chem. 2021, 60, 8011−8026